Fast synaptic transmission in the goldfish CNS mediated by multiple nicotinic receptors

Charlotte L. Grove[1], Theresa M. Szabo[1,2], J. Michael McIntosh[3], Samantha C. Do[1], Robert F. Waldeck[4] and Donald S. Faber[1]

[1] *Dominick P. Purpura Department of Neuroscience, Albert Einstein College of Medicine, Bronx, NY 10461, USA*
[2] *Department of Biological Sciences, Delaware State University, Dover, DE 19901, USA*
[3] *Departments of Biology and Psychiatry, University of Utah, Salt Lake City, UT 84112, USA*
[4] *Neuroscience Program and Department of Biology, University of Scranton, Scranton PA 18510, USA*

The Journal of Physiology

Non-technical summary Usually nicotinic receptors in the central nervous system only influence the strength of a signal between neurons. At a few critical connections, for instance some of those involved in the flight response, nicotinic receptors not only modulate the signal, they actually determine whether a signal is conveyed or not. We show at one of the few such connections accessible for study, up to three different nicotinic receptor subtypes mediate the signal. The subtypes appear to be clustered in separate locations. Depending on the number and combination of the subtypes present the signal can range from short to long duration and from low to high amplitude. This provides a critical connection with a built-in plasticity and may enable it to adapt to a changing environment.

Abstract In this study, fast synaptic transmission at vertebrate CNS connections mediated by several different nicotinic ACh receptors (nAChRs) was investigated with paired recordings from pre- and postsynaptic neurons. Analysis of the response kinetics at the axo-axonic connections between the Mauthner (M-) axon and cranial relay neurons (CRN) indicates up to three main components are present and can be characterized by fast, $\sim$1.5 ms, intermediate, $\sim$6 ms and slow, $\sim$15 ms, decay time constants. Further analysis indicates most responses have multiexponential decays and each response falls into one of six classes dependent on the weight and combination of kinetic components. Pharmacological results suggest that up to three nAChRs, $\alpha7^*$, $\alpha3\beta2^*$ and $\alpha3\beta4^*$, mediate the postsynaptic responses and correspond to the fast, intermediate and slow decay components, respectively. The fast decay component is blocked by $\sim$35 nM methyllycaconitine (MLA), 100 nM α-bungarotoxin (α-Btx) or 150 nM α-conotoxin (α-Ctx) ArIB. The intermediate decay component is blocked by 2 μM dihydro-beta-erythroidine (DHβE) or 200 nM α-Ctx GIC. The slow decay component is blocked by 10 μM α-Ctx AuIB, but not by 7.25 μM DHβE. Intriguingly, the mEPSPs (minis) at connections with evoked EPSPs best fitted by multiple exponentials, were not composite; rather, there were multiple populations of minis, each with single exponential decay times corresponding to those of the different evoked EPSP components. This indicates that the different receptors are topographically segregated at the connection between the M-axon and CRN axon. These results suggest that, as with glutamate, fast nicotinic synaptic transmission in the CNS can be mediated by multiple receptors in the same postsynaptic neuron. The coexistence of EPSPs of different durations may have implications for network function and plasticity.

Introduction

Nicotinic transmission is widespread in both the central and autonomic nervous systems and most studies have focused on the modulatory role of nicotinic ACh receptors (nAChRs), largely because there are relatively few examples of their postsynaptic function (McGehee *et al.* 1995; Jones *et al.* 1999; Berg & Conroy, 2002; McIntosh *et al.* 2005; Wonnacott *et al.* 2006; Dani & Bertrand, 2007). Unfortunately, models of fast nicotinic transmission in the CNS have not been accessible for paired recordings (Roerig *et al.* 1997; Frazier *et al.* 1998; Alkondon *et al.* 1998; Nong *et al.* 1999; Bradaia & Trouslard, 2002; Hatton & Yang, 2002; Guo *et al.* 2005; Thinschmidt *et al.* 2005). A notable exception is the nicotinic axo-axonic connection between the Mauthner (M-) axon and cranial relay neuron (CRN) of the goldfish, which is readily accessible for paired recordings and pharmacological manipulations. As this is an *in vivo* model, correlations between behaviour and physiology are also feasible (Weiss *et al.* 2006).

Key insights into the physiology of $\alpha7$ and non-$\alpha7$ nACh receptors have come from paired recordings in dissected chick ciliary ganglion of the autonomic system. There, fast synaptic transmission (Zhang *et al.* 1996; Ullian *et al.* 1997) is mediated by $\alpha7$ nAChRs, concentrated on spines and largely excluded from postsynaptic densities (PSDs), and by $\alpha3^*$ nAChRs, where * indicates the possible presence of additional subunits (Lukas *et al.* 1999), located within somatic PSDs (Jacob & Berg, 1983; Jacob *et al.* 1984; Loring *et al.* 1985; Horch & Sargent, 1995; Williams *et al.* 1998; Shoop *et al.* 1999). The means by which $\alpha7$ nAChRs are activated is debated. Possible contributions to the $\alpha7$ nAChR response include (1) acetylcholine release at sites not apposed to PSDs, that is, ectopic release on spines (Shoop *et al.* 1999, 2001; Coggan *et al.* 2005; Sargent, 2009), (2) multiquantal release at the relatively rare spinous active zones and/or (3) diffusion of transmitter released somatically to PSDs on spines (Nguyen & Sargent, 2002). These observations raise the question of the functional organization of fast nicotinic synapses in the vertebrate CNS.

To study fast nicotinic transmission we have used an *in vivo* CNS model system, the connection in the goldfish hindbrain between the M-axon and the post-synaptic CRNs. The M-cell is responsible for a stereotyped escape behaviour in the goldfish, the C-start (Zottoli, 1977). CRNs relay the command from the M-axon to motorneurons controlling jaw, opercular and ocular muscles (Diamond, 1971; Hackett & Faber, 1983*a*; Hackett & Buchheim, 1984) and to interneurons that mediate feedback inhibition of the M-cells (Hackett & Faber, 1983*b*). Based on morphology, at least two classes of CRNs have been reported. In one class, the axon projects medially from the cell body, crosses over the nearest M-axon and midline before projecting only rostrally to innervate the trigeminal nucleus (Hackett & Buchheim, 1984). In another class, CRN axons bifurcate and course both rostrally and caudally after crossing the midline (Titmus & Faber, 1987). By inspection of the CRN homologues in the zebrafish (Kimmel *et al.* 1985), the T-reticular interneurons, coupled with the morphological evidence in the goldfish, it is likely that different types of CRNs serve different motoneuron targets. The homologue of the M-axon–CRN connection in the hatchetfish is the nicotinic connection between the Mauthner and giant fibres, which controls pectoral fins in addition to the aforementioned targets (Auerbach & Bennett, 1969).

We have used the M-axon–CRN connection to investigate fast nAChR-mediated transmission in the CNS and the properties imparted by distinct nAChR subtypes. We found that the postsynaptic receptor complement is diverse and can include combinations of $\alpha7^*$ and non-$\alpha7$ nAChRs, which produce different decay kinetics in the EPSPs among CRN types. Furthermore, electrophysiological data indicate these receptor subtypes are localized to separate clusters, possibly within one contact or on the separate distinct contacts that comprise a connection. This insight lays the foundation for studying the functional contributions of the different receptor subtypes and pre- and postsynaptic factors influencing the strength and dynamics of the EPSP.

Methods

Ethical approval

All experiments were performed in accordance with the Institutional Animal Care and Use Committee (IACUC) protocols approved at Albert Einstein College of Medicine, consistent with the National Institutes of Health's Guide for the Care and Use of Laboratory Animals and compliant with all federal, state and local regulations.

Surgery

One hundred adult male or female goldfish (*Carassius auratis*, length 7.5–10 cm, measured without the tail) were obtained from EECHO Systems (North Kansas City, MO, USA), Hunting Creek Fisheries (Thurmond, MD, USA) and Billy Bland Fisheries (Taylor, AR, USA), and were maintained in conditioned water at 17–18°C (Szabo *et al.* 2006). Goldfish were anaesthetized using 60 mg l^{-1} 3-aminobenzoic acid ethyl ester (MS222) in conditioned water and subsequently mounted in an experimental chamber in which animals were respirated through the mouth to provide a continuous flow of aerated conditioned water over the gills. This water contained 60 mg l^{-1} MS222 and was cooled to 6°C. The spinal cord was exposed for antidromic stimulation of the M-cell

and goldfish were immobilized with d-tubocurarine chloride (Abbot Laboratories, Chicago, IL, USA) injected intramuscularly (1 mg (gm body weight)$^{-1}$) after the anaesthesia took effect. The cranium was opened dorsally at the location of the fourth ventricle and the cerebellum and the facial lobes were gently retracted rostrally and retained with paper spatulas fashioned from Kimwipes (Mississauga, Ontario, Canada). Subsequently, the vagal lobes were retracted laterally and retained to reveal the section of the brainstem containing the CRN cell bodies and to enable placement of electrodes in the M-axon and CRN as illustrated in Fig. 1 (Faber & Korn, 1978; Waldeck *et al.* 2000). At the end of the experiment, the goldfish used for this project were killed by decapitation in accordance with IACUC protocols.

Electrophysiology

Paired recordings from the M-axon and CRN axon were made in current clamp mode using sharp electrodes and an Axoprobe (Axon Instruments, Foster City, CA, USA), a two-electrode amplifier with cross talk neutralization. The presynaptic electrodes were filled with 3 M KCl buffered with 10 mM Hepes, pH 7.2 (resistance 8–11 MΩ). The postsynaptic electrodes were filled with 3 M KCl, 75 mM *N*-(2,6-dimethylphenylcarbamoylmethyl)triethyl-ammonium bromide (QX-314) and 2.5% neuro-biotin (resistance 14–18 MΩ). QX-314 eliminated contamination by regenerative sodium-dependent responses during collection of EPSPs that were otherwise suprathreshold at low stimulus frequency. The presynaptic M-axon, a myelinated axon 70–100 μm in diameter situated 100–200 μm from the midline and at most 100–150 μm below the hindbrain surface, was penetrated after being located with the aid of a stereomicroscope. The CRN axons, which run alongside and within 50 μm of the M-axon in the hindbrain, were found by systematically probing the hindbrain while stimulating the M-axon antidromically with an electrode on the exposed caudal spinal column. Once a postsynaptic CRN was penetrated, the M-axon was stimulated with transmembrane current pulses (15–30 nA, 18 ms duration). The identity of a CRN was confirmed by the rapid depression of its response to repeated M-axon stimulation, evidence of inputs from both M-axons, the EPSP waveform and monosynaptic latency (Hackett & Faber, 1983*a*; Hackett *et al.* 1989; Waldeck *et al.* 2000).

Miniature EPSPs (mEPSPs) were collected continuously at a 60 μs per point sampling rate, first without depolarization and subsequently with a 10–20 nA depolarization of the M-axon. Asynchronous mEPSPs rarely followed the large stimulus-evoked responses. Without depolarization spontaneous mEPSPs frequency was 1.8 ± 1.3 events s^{-1} ($n = 6$).

Perfusion of drugs

The brain was superfused with normal fish saline (in mM: 124.0 NaCl, 5.1 KCl, 2.8 NaH$_2$PO$_4$.H$_2$O), 0.9 MgSO$_4$, 1.6 CaCl$_2$.2H$_2$O, 5.6 glucose and 20.0 Hepes, pH 7.2), and the perfusate was drained continuously via a shunt posterior and lateral to the hindbrain. Two protocols were employed for delivery of antagonists to the hindbrain. α-Conotoxins (α-Ctx) GIC, AuIB and ArIB were injected via a septum into the fish saline superfusion stream, which was maintained at 6°C and flowed at a rate of 30 μl min^{-1}. A bolus of α-Ctx (20–50 μl) was injected over 1 min. A 0.5 ml volume between the injection site and the point at which the superfusion was delivered to the brain surface enabled adequate mixing of antagonist before the delivery point to provide consistent results. This arrangement enabled a reasonably rapid delivery and exchange of drugs, with minimum consumption of antagonist and minimum mechanical disruption at the brain surface. A higher perfusion flow rate (150–250 μl min^{-1}) protocol, which provided even greater stability and enabled longer recording times, was used to deliver: α-Btx (Tocris, Ellisville, MO, USA), DHβE and MLA. Unless otherwise specified, chemicals and reagents were purchased from Sigma (St Louis, MO, USA). α-Ctxs were provided by J. M. McIntosh and synthesized as previously described: ArIB (Whiteaker *et al.* 2007), AuIB[V11L;V16D] (Luo *et al.* 1998) and GIC (McIntosh *et al.* 2002).

Neurobiotin injection and immunohistological protocol

In some experiments, after gathering electrophysiological data the morphology of the M-axon–CRN connection was marked by injecting Neurobiotin (Vector Laboratories, Burlingame, CA, USA). The marker was injected iontophoretically into the CRN for at least 30 min using 90 nA depolarizing current injections (400 ms at 1 Hz). Subsequently, the fish was perfused intracardially with phosphate buffer and 4% paraformaldehyde in PBS, pH 7.4. The dissected brain was refrigerated in fresh 4% paraformaldehyde for 24 h, transferred to cryoprotectant (30% sucrose in 0.1 M phosphate buffer) and stored at 4°C. Using a CM3050S cryostat (Leica Microsystems, Nussloch, Germany), 60 μm horizontal slices were made and retrieved in a 24-well plate containing 0.1 M phosphate buffer and refrigerated until further processing. Slices were washed in 0.5% Triton in 0.1 M phosphate buffer and treated for 1 h in a blocking solution containing 10% normal goat serum (Jackson ImmunoResearch, West Grove, PA, USA). Brain sections were incubated overnight in primary antibodies to zonula occludins II (rabbit anti-ZO-2) (Molecular Probes, Eugene, OR, USA) at a 1:125 dilution in 0.5% Triton and 5% normal goat serum in PBS at 4°C. ZO-2 antibodies were used because they

have been shown to selectively stain the M-axon (Flores *et al.* 2008). To image the CRN injected with Neurobiotin, sections were incubated for 2 h at room temperature in streptavidin AlexaFluor 488 (Molecular Probes) at a 1:250 dilution. At the same time secondary antibodies conjugated to AlexaFluor goat anti-rabbit (Molecular Probes) at a 1:250 dilution were added to visualize the M-axon. AlexaFluor conjugated α-bungarotoxin was used to mark the putative $\alpha7^*$ acetylcholine receptors located at the M-axon–CRN connection.

Serial sections were analysed and images were recorded with an upright Olympus BX61WI and Zeiss LSM 5 Duo V2 confocal microscopes of the Morphology and Image Analysis Facility of the Kennedy Center at Albert Einstein College of Medicine. FluoView and Imaris software were used to create projection images.

Data analysis

Custom software (Trace Analyzer 2 and 3) was used to collect data and analyse EPSP amplitudes. The sampling rate for EPSPs and mEPSPs were 10–25 μs point^{-1} and 60 μs point^{-1}, respectively. Artifacts caused by current injection on the tails of some EPSPs were removed from the traces. Decay times were analysed using Igor (Wavemetrics, Lake Oswego, OR, USA) and Detectivent (Ankri *et al.* 1994). To improve the signal-to-noise ratio 5–20 EPSP traces were averaged for decay time analysis. Only data taken under steady-state conditions were averaged, and only one frequency was used during a given experiment, and therefore skewing the relative amplitudes of the different components as a function of changing depression was avoided. Decay time constants of EPSPs were determined by fitting the decaying phase initially with a single exponential and then increasing to the optimum number of exponentials as determined by the *F* test and *P* value $\leq$ 0.05. The robustness of each fit was explored by varying the initial conditions up to one order of magnitude from time constants determined by the initial fit and by increasing the width of the fitting window in increments by 20 ms.

Only the EPSP decays best fitted by a combination of four time constants, $\tau1$–$\tau4$ (class 6), exhibited sensitivity to the width of the fit windows and the initial conditions. For the cases in which one component had been isolated or determined as a difference peak by using antagonists, the exponential fit of the composite peak that contained the time constant that most closely matched that of the isolated single component was selected. If such an empirical constraint was not available, the average values for $\tau1$–$\tau4$ were used (Table 1).

To ensure that the mEPSPs were detected without bias, measurements were automated. Detectivent software was used to detect randomly occurring mEPSPs and

analyse mEPSP decay time constants. Initially mEPSPs were treated as monoexponential. The resulting decay time constant distributions ranged from mono- to trimodal and could be fitted with sums of Gaussians. These decay times were confirmed using Igor software. Origin 7 (Northampton, MA, USA) was used to construct the decay time distributions. Averaging of mEPSPs was used to improve the signal-to-noise ratio (Zhang *et al.* 1996). For averaging, between 20 to 50 mEPSPs from each population defined by a mode and within 3 standard deviations of each Gaussian mean were selected. mEPSPs were aligned by their rising edges. Events with amplitudes of less than three times the standard deviation of the noise or with tails or onsets overlapping another mEPSP were not used in the averaged data.

Basic logical alignment search tool (BLAST) and vector alignment search tool (VAST) available at the National Center for Biological Information were used to compare sequence and structural identity of $\alpha3$, $\alpha7$, $\beta2$ and $\beta4$ nAChRs across species.

Results

Data from CRNs in the goldfish (Hackett and Faber, 1983*a*) and their homologues in hatchetfish (Model *et al.* 1975; Gilat *et al.* 1986; Barry & Bennett, 1990) and zebrafish (Kimmel *et al.* 1985) indicate each CRN receives inputs from both M-axons via axo-axonic contacts. The CRN axons are $\sim$20 μm in diameter and are myelinated (Hackett & Buchheim, 1984). As shown schematically in Fig. 1, there are a limited number of axo-axonic contacts between short collaterals issued by both the Mauthner and CRN axons (Hackett & Buchheim, 1984; Waldeck *et al.* 2000). For clarity only, one CRN on one side of the midline is illustrated. Because of their axonal location, the contacts comprising this connection represent the dominant input to the CRN. Both pre- and postsynaptic elements are accessible for intracellular physiology, and the large visible M-axon enables manipulations designed to elucidate pre-synaptic factors influencing synaptic transmission. Since the connections are axo-axonic, it is possible to detect and analyse mEPSPs largely uncontaminated by non-M-axon inputs (Barry & Bennett, 1990; Waldeck *et al.* 2000).

In the electrophysiological context, the M-axon that is immediately adjacent to the rostral–caudal or parallel branch of the CRN is termed the ipsilateral M-axon. Since the M-axons decussate, the CRN and Mauthner cell bodies are on the same side of the hindbrain. Typical contact locations, one between the crossing CRN branch and contralateral M-axon and several between the parallel CRN branch and ipsilateral M-axon, are indicated in Fig. 1, centre panel. Contacts from the ipsilateral M-axon are most often observed within $\sim$200 μm of crossing branch of the CRN axon. A confocal image shows a typical

Table 1. Decay kinetics of EPSPs

	n	Rel. Wt	$\tau 1$ (ms) *Rel. Wt*	$\tau 2$ (ms) *Rel. Wt*	$\tau 3$ (ms) *Rel. Wt*	$\tau 4$ (ms) *Rel. Wt*
Class 1 $\alpha 7^*$						
$\tau < 2.20$	48		1.4 ± 0.3 *88.6 ± 3.6%*	14.4 ± 9.2 *11.4 ± 3.6%*		
All class 1	75	54.7%	1.7 ± 0.4 *87.9 ± 4.3%*	15.7 ± 10.0 *12.1 ± 4.3%*		
Class 2 $\alpha 3\beta 2^*/\alpha 3\beta 4^*$						
All class 2	6	4.4%			5.3 ± 1.3 *42.7 ± 24.1%*	14.7 ± 4.2 *57.3 ± 24.1%*
Class 3 $\alpha 3\beta 4^*$						
All class 3	4	2.9%				9.0 ± 1.6 *100.0%*
Class 4 $\alpha 7^*/\alpha 3\beta 2^*$						
2 kinetic components	5		1.7 ± 0.3 *52.2 ± 24.9%*		6.2 ± 1.6 *47.8 ± 24.9%*	
3 kinetic components	7		1.4 ± 0.2 *72.5 ± 15.7%*	22.0 ± 4.9 *10.4 ± 4.8%*	4.3 ± 1.0 *17.1 ± 12.6%*	
All class 4	12	8.8%	1.5 ± 0.3 *64.1 ± 21.7%*	22.0 ± 4.9 *6.1 ± 6.4%*	5.1 ± 1.6 *29.9 ± 23.7%*	
Class 5 $\alpha 7^*/\alpha 3\beta 4^*$						
2 kinetic components	23		1.8 ± 0.4 *51.9 ± 23.9%*	13.2.0 ± 4.2** *6.4 ± 3.0%***		13.2 ± 4.2** *41.7 ± 26.8%***
3 kinetic components	2		1.8 ± 0.4 *76.9 ± 2.9%*	15.7 ± 10.0 *8.5 ± 3.2%*		13.2 ± 2.2 *14.6 ± 6.1%*
All class 5	25	18.2%	1.8 ± 0.4 *53.8 ± 23.9%*	13.4 ± 4.6 *6.6 ± 3.0%*		13.2.0 ± 4.1 *39.6 ± 26.8%*
Class 6 $\alpha 7^*/\alpha 3\beta 2^*/\alpha 3\beta 4^*$						
3 kinetic components	11		1.7 ± 0.5 *23.9 ± 10.7%*	16.3 ± 4.1*** *2.9 ± 1.3%***	6.2 ± 1.3 *40.0 ± 1.4%*	16.3 ± 4.1*** *33.2 ± 16.5%***
4 kinetic components	4		1.6 ± 0.6 *26.2 ± 10.9%*	22.3 ± 13.3 *5.1 ± 0.7%*	5.0 ± 2.1 *37.0 ± 17.3%*	10.5 ± 1.3 *31.6 ± 16.6*
All class 6	15	10.9%	1.6 ± 0.5 *24.5 ± 10.4%*	17.9 ± 7.6 *3.5 ± 1.5%*	5.9 ± 1.5 *39.2 ± 14.0%*	14.8 ± 4.4 *32.8 ± 16.0%*
All classes	137					
Classes blocked/isolated						
Class 1	9		1.6 ± 0.2	13.4 ± 8.0		
Class 2	4				6.0 ± 1.7	
Class 2, 3 & 6	6					13.2 ± 3.8

Within tau group and across classes, *t* test $P > 0.05$, except $\tau 4$ of class 3, which is significantly different from $\tau 4$ for all other associated classes, *t* test $P < 0.05$; ** and *** indicate that the t2/t4 component has been partitioned between $\tau 2$ and $\tau 4$ class 5 (**) and class 6 (***).

junction between the M-axon and CRN axon collaterals (Fig. 1, lower left). In the goldfish (Hackett *et al.* 1989) and in the hatchetfish (Model *et al.* 1975), each contact contains multiple active zones. Transmission between the M-axon and a CRN is blocked by d-tubocurarine and is believed to be cholinergic based on this finding and on the observation of α-Btx staining in the hatchetfish (Day *et al.* 1983).

Paired recordings were obtained with the pre- and postsynaptic electrodes placed within the confines of the vagal lobe, and we estimated that the CRN electrode was typically within 200 μm of the contact zone (Fig. 1).

EPSPs were triggered by a spike, which was evoked by a brief depolarizing current pulse in the recorded M-axon. M-axon spike height and duration were monitored throughout the experiment. We estimated that the CRN axon length constant and effective membrane time constant were $\sim$2 mm and $\sim$400 μs, respectively, on the basis of paired simultaneous recordings from single CRN axons, while applying 7 nA through one electrode in two preparations. This time constant was faster than the decay time of any EPSP component described in the present work. For EPSP components with decay time constants >2 ms, it was unlikely that either the size or kinetics of the

spontaneous and evoked EPSPs were appreciably degraded by CRN cable properties. Although some degradation may have occurred with EPSPs components having decay time constants of ~1.5 ms, it was still possible to correlate kinetics and pharmacology.

EPSP kinetics

Data collected from 137 M-axon–CRN axon pairs exhibited a wide range of the evoked EPSP decay kinetics. This was quantified by inspection of the distribution of decay time constants, obtained by assuming mono-exponential decay (Fig. 2). On this basis, the decay time constant ranged from ~1 ms to 12 ms, i.e. over one order of magnitude. As shown in Fig. 2, at least one clear population of EPSPs could be distinguished on this basis, with $\tau_{mean} = 2.1 \pm 0.5$ ms. Subsequently, we asked if each EPSP decay could be better fitted as a multiexponential, using the F test to establish the optimum number of decay components. On this basis, the EPSPs fell into six different classes characterized by some combination of up to four time constants, $\tau 1$–$\tau 4$. The following combinations exist: class 1: $\tau 1$ and $\tau 2$; class 2: $\tau 3$ and $\tau 4$; class 3: $\tau 4$ only; class 4: $\tau 1$, $\tau 2$ and $\tau 3$; class 5: $\tau 1$, $\tau 2$ and $\tau 4$; and class 6: $\tau 1$, $\tau 2$, $\tau 3$ and $\tau 4$. Among the exemplars from each class (Fig. 2) only
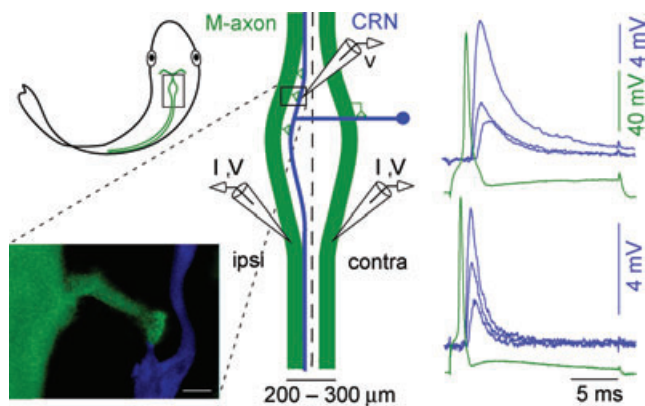

Figure 1. Characteristics of the excitatory axo-axonic connection between the Mauthner (M-) and cranial relay neuron (CRN) axons
Location of M-axon–CRN connection in goldfish hindbrain is highlighted with a rectangle (upper left). For clarity only one CRN is illustrated and as indicated, a CRN receives input from both M-axons. Expanded diagram (centre) depicts the typical contact locations (triangles) between a presynaptic M-axon (green) and a postsynaptic CRN axon (blue). M-axons 50–100 μm in diameter run within 75–400 μm of each other and parallel to the midline (dashed line). The lower left panel shows a confocal image of a M-axon (green)–CRN (blue) axo-axonic contact. The calibration bar is 20 μm. Right, current pulses (*I*) injected into either the ipsilateral or contralateral M-axon generate a presynaptc action potential followed by EPSPs that depress with increasing stimulus number (1, 2 and 10) at 1 Hz. The EPSP decay kinetics differ among CRNs and can range from slow (upper right) to fast (lower right).

the class 3 EPSP is well fitted by one exponential using the F test criterion. The average values and weight of the decay time constants and the relative prevalence of class type are listed in Table 1. The EPSPs with values of $\tau 1$–$\tau 4$ blocked or isolated by antagonists are also listed in Table 1.

As mentioned, only one distinct mode is present in the histogram of decay time values (Fig. 2). A total of 48 EPSPs in the first mode of the histogram, which are termed class 1 EPSPs, are well separated from the right shoulder of this mode and are best fitted by two time constants, $\tau 1$: 1.4 ± 0.3 ms and $\tau 2$: 14.4 ± 9.2 ms with relative weights of $88.6 \pm 3.6\%$ and $11.4 \pm 3.6\%$, respectively (Table 1). We chose this subset, 48 of the 75 EPSPs comprising this distinct mode, to avoid the overlap region between class 1, 4 and 5 EPSPs. The dominant time constant, $\tau 1$, is the fastest decaying of the four time constants observed. In 8.9% of the cases, class 4 EPSPs, there was a third, inter-mediate component, with $\tau 3 \approx 5$–6 ms, in combination with $\tau 1$ and $\tau 2$. In 18.2% of the responses, class 5 EPSPs, the contribution of a slowly decaying component, $\tau 4 \approx 14$ ms, is observed in combination with $\tau 1$ and $\tau 2$. Note that although $\tau 4$ and $\tau 2$ have similar values, they are associated with different receptor types as will be clarified by the pharmacological data. Finally, in 10.9% of the responses, class 6 EPSPs, both the intermediate and slowly decaying components are present along with $\tau 1$ and $\tau 2$ components. Thus, the majority of the EPSPs have $\tau 1$ and $\tau 2$ components, in isolation or in combination with the other taus, and we focused first on the characterization of this primary response.

Fast kinetic decay: EPSP class 1

The majority of CRNs, 85%, were investigated by stimulating the ipsilateral M-axon, thus probing connections with multiple contacts. Including these, as well as responses to input from contralateral M-axons, EPSPs from class 1 were observed 53.7% of the time. As nicotinic antagonists can block transmission at the M-axon–CRN connection and its homologue in the hatchetfish (Model *et al.* 1972; Day *et al.* 1983), we asked if the responses could be attributed to the nAChRs.

In the example of Fig. 3*A* the decay of a class 1 EPSP was fitted by a double exponential with time constants of 1.7 and 19.3 ms for $\tau 1$ and $\tau 2$, respectively, and the EPSP was completely blocked by 200 nM MLA. Overall, we found that EPSPs of this class are blocked by ~35 nM MLA, as shown in the dose–response curve representing the results from 10 M-axon–CRN pairs at nine concentrations of MLA, $n = 2$ for 10 nM MLA (Fig. 3*B*). The inset is an example of the block at 35 nM MLA. As discussed below, this suggests that class 1 EPSPs are mediated by $\alpha 7^*$ nAChRs (Alkondon & Albuquerque, 1993). Access of antagonists to the M-axon–CRN connection in the *in*

vivo preparation may be more limited than to nicotinic connections that have been investigated in slice and culture preparations in other species or to nAChRs expressed in oocytes. As 35 nM MLA can take more than 1 h to completely block the response, concentrations of 100–200 nM MLA were routinely used to reduce the time to block to ~30 min.

To confirm that the two decay time constants characterizing class 1 EPSPs can both be attributed to $\alpha7^*$ nAChRs, we compared the waveforms of the EPSPs at different stages of the block. Figure 3*Ca* illustrates the time course of antagonism by 200 nM MLA; the EPSP was reduced by ~40% and 70% from control (point 1) at points 2 and 3, respectively. In Fig. 3*Cb* the corresponding EPSPs are normalized to match the size of the control, and the superimposed responses demonstrate that all three EPSPs have the same waveform. Class 1 EPSPs were also blocked by 50–100 nM α-Btx, an $\alpha7$ nAChR antagonist (Zhang *et al.* 1994). Finally, to further establish that goldfish class 1 EPSPs are mediated by $\alpha7^*$ nAChRs, we used 150 nM α-Ctx ArIB[V11L;V16D], a highly specific $\alpha7$ nAChR antagonist (Whiteaker *et al.* 2007), to block class 1 EPSPs (Fig. 3*D*).

Intermediate and slow kinetic decay: EPSP classes 2 and 3

Two classes associated with two additional time constants, $\tau3$ and $\tau4$, were identified from decay time analysis (Fig. 2,

and Table 1). The EPSPs in class 2 are best fitted by intermediate, $\tau3$, and slow, $\tau4$, time constants, while those in class 3 are fitted by only the slow time constant, $\tau4$. In class 2 the average values and relative weights for $\tau3$ and $\tau4$ are 5.3 ± 1.3 ms, $42.7 \pm 24.1\%$ and 14.7 ± 4.2 ms, $57.3 \pm 24.1\%$, respectively, and $\tau4$ has a value of 9.0 ± 1.6 for EPSPs in class 3 (Table 1). Although EPSP classes 2 and 3 accounted for only 7% of all pairs studied, the components, $\tau3$ and/or $\tau4$, are present in five of the six classes observed. Overall these components are found in 45% of the EPSPs.

As all time constants identified in this study are represented in EPSP classes 1–3, primarily these classes were used for the pharmacological studies. As just discussed, class 1 EPSPs, associated with $\tau1$ and $\tau2$, are mediated by $\alpha7^*$ nAChRs. We next asked if non-$\alpha7$ nAChRs mediated the EPSP components associated with the intermediate and slow time constants, $\tau3$ and $\tau4$. In class 2 EPSPs the weight of each of the components, $\tau3$ and $\tau4$, is large enough to be readily detected and only one time constant, $\tau4$, is associated with class 3 EPSPs, making these classes advantageous for the pharmacological experiments.

In contrast to class 1 EPSPs, pharmacological evidence suggested that two receptor subtypes mediate a class 2 EPSP. In the example of Fig. 4*A*, the control EPSP decay was fitted as the sum of two exponentials, $\tau3 = 4.9$ ms and $\tau4 = 12.8$ ms. This EPSP was partially blocked by 1.5 μM MLA and the residual response decayed
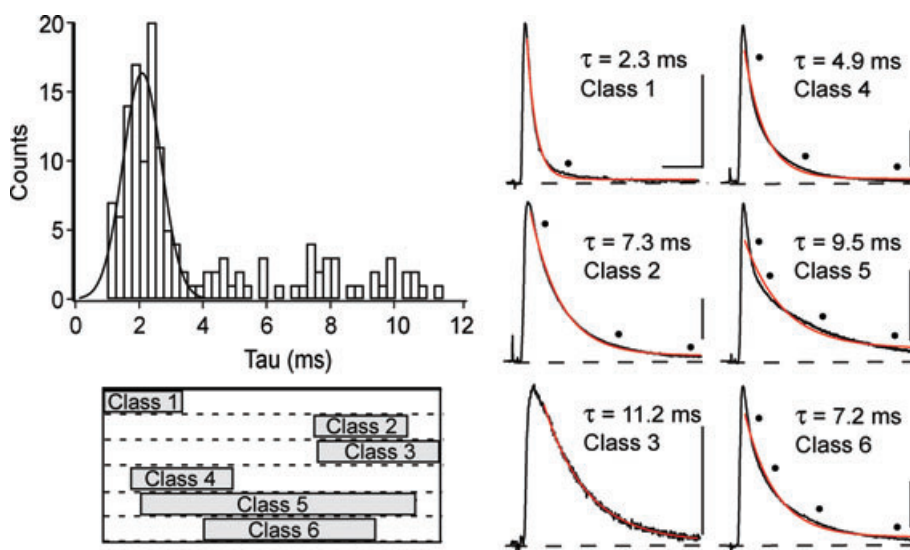

Figure 2. Decay time histogram of M-axon–CRN pairs
The decay phase of 137 EPSPs were fitted with one exponential. One distinct mode representing class 1 EPSPs is present in the histogram with a mean at 2.1 ms. Exemplars of the single exponential fits of classes 1–6 EPSPs, illustrate that these EPSPs will best be fitted by more than one exponential, except for the class 3 EPSP, which is well fitted with one exponential. Dots mark the points of divergence between the trace and the fit. EPSP classes 1, 4, 5 and 6 represent the majority of all EPSPs recorded. The width of the decay time windows associated with all EPSP classes, 1–6, are indicated by bars below the histogram. Horizontal calibration bar, 10 ms, applies to all classes. Vertical calibration bars, 2 mV for class 3 and 4 mV for all other classes.

monoexponentially with a time constant, $\tau 4$, of 13.5 ms, similar to that extracted from the fit of the composite control. To minimize access time, 1.5–2 μM MLA routinely was used to block the signal associated with $\tau 3$ time constant. The residual response, i.e. that associated with $\tau 4$, is insensitive to MLA at concentrations as high as $\sim$20 μM. In Fig. 4*A* the difference signal, i.e. the MLA-sensitive component, had a decay time constant of 4.5 ms, a value within the $\tau 3$ range (Table 1).

The $\tau 3$ component was also blocked by 2 μM DHβE (Fig. 4*B*) and by 200 nM α-Ctx GIC (Fig. 4*C*). Taken

together, these data suggest that the $\tau 3$ response is mediated by $\alpha 3\beta 2^*$ nAChRs. In other systems, $\alpha 3\beta 2^*$ nAChRs were blocked by $> 1 \mu$M MLA (Drasdo *et al.* 1992; Astles *et al.* 2002) or by 1–1.6 μM DHβE (Chavez-Noriega *et al.* 1997; Faria *et al.* 2003). α-Ctx GIC is a peptide that blocks nAChRs in the sequence $\alpha_3\beta_2 \gg \alpha_4\beta_2 > \alpha_3\beta_4$. At 100 nM, α-Ctx GIC completely blocks human $\alpha 3\beta 2$ expressed in oocytes (McIntosh *et al.* 2002), and it also blocks $\alpha 6\beta 2^*$ nAChRs (J. M. McIntosh, unpublished observation); since 200 nM MLA can block $\alpha 6\beta 2^*$ nAChRs in rat (Mogg *et al.* 2002), the contribution
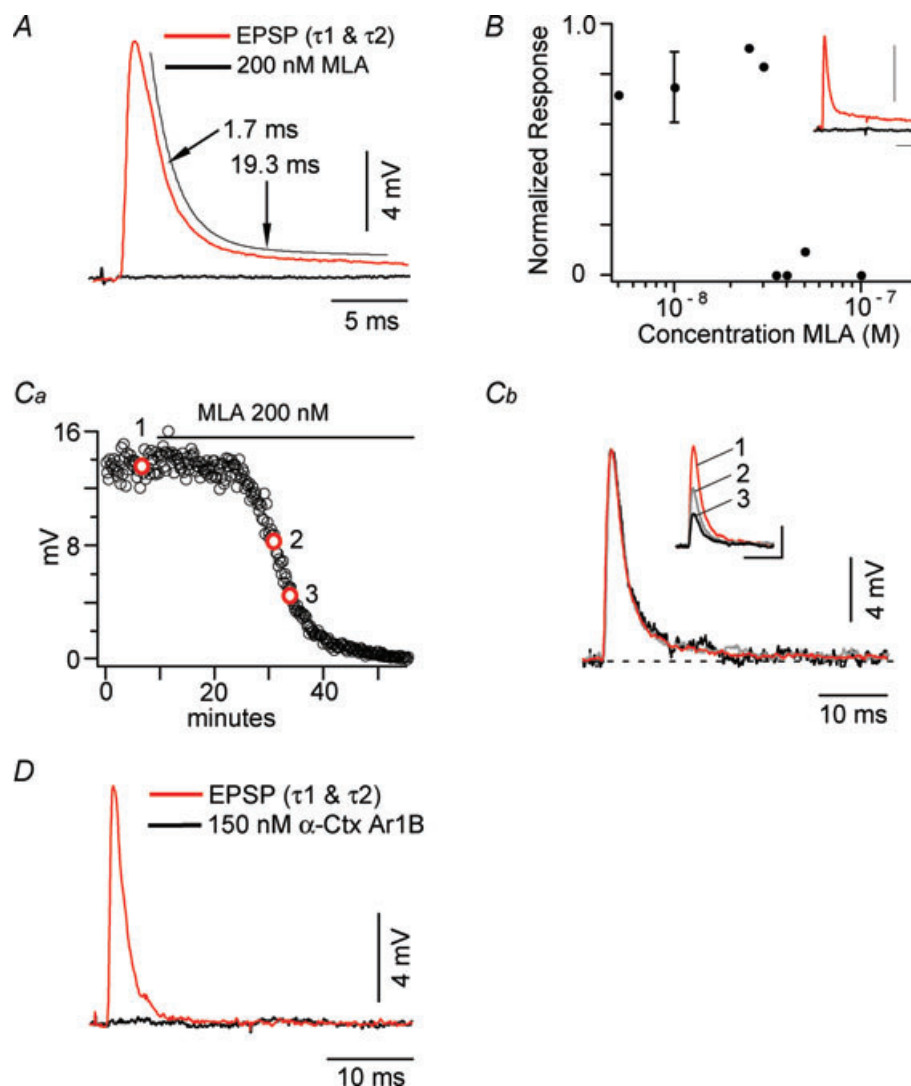

Figure 3. MLA and α-Ctx ArIB block class 1 EPSPs
A, class 1 EPSP obtained before (red) and after (black) superfusion with 200 nM MLA. The decay of the control EPSP is fitted as the sum of two exponentials (offset thin black line), with $\tau 1 = 1.7$ ms and $\tau 2 = 19.3$ ms. *B*, dose–response curve for MLA. Inset shows block of class 1 EPSP with 35 nM MLA. Calibration bars are 10 ms and 4 mV. *C*, time course of MLA block. *Ca*, plot of EPSP amplitude *vs.* time in the same experiment as in *A* (frequency: 0.08 Hz). Red circles 1, 2 and 3 refer to time points at which responses in *Cb* were obtained. *Cb*, EPSPs from time points before MLA (1 – red, control), after $\sim$40% block (2 – grey) and after $\sim$70% block (3 – black) are scaled to the control EPSP and superimposed, showing both exponentials, $\tau 1$ and $\tau 2$, are equally sensitive to the antagonist. Inset shows the unscaled EPSPs. Calibration bars pertain to the unscaled data. *D*, class 1 EPSP obtained before (red) and after (black) superfusion with 150 nM α-Ctx ArIB [V11L;V16D].

of $\alpha6\beta2^*$ nAChRs has not yet been ruled out in class 2 EPSPs.

In Fig. 4A–C, the EPSP component remaining in the presence of MLA, DHβE or α-Ctx GIC has a decay time constant ranging from 13.2–20.2 ms, i.e. $\tau4$. Because of the relatively slow decay associated with this component, we asked if it could be mediated by $\alpha3\beta4^*$ nAChRs. Relative to the decay kinetics of $\alpha7$ and $\alpha3\beta2$ nAChRs expressed in oocytes, those of $\alpha3\beta4$ AChRs are slow (Chavez-Noriega *et al.* 1997). The $\tau4$ component was blocked completely by 10 μM α-Ctx AuIB (Fig. 4D). At 10 μM α-Ctx AuIB antagonized responses of rat $\alpha3\beta4$ nAChRs expressed in oocytes (Luo *et al.* 1998), of rat major pelvic ganglion neurons (Park *et al.* 2006), and of chick ciliary ganglion neurons (Nai *et al.* 2003) by 80–95%. Additionally, a slow decay of a nAChR EPSP is consistent with the presence of a heteromer containing $\beta4$ subunits (Figl & Cohen, 2000).

MLA is primarily used as an $\alpha7$ nAChR antagonist. However, it partially blocks ($\sim$57 to 95%) $\alpha3\beta4$ nAChRs in a number of species at concentrations approximately three orders of magnitude greater than that used for $\alpha7$ nAChRs (Fucile *et al.* 1998; Lopez *et al.* 1998; Astles *et al.* 2002; Bryant *et al.* 2002). In our experiments with the goldfish $\sim$20 μM MLA has no effect on the $\tau4$ component. However, the identification of the $\tau4$ component as an $\alpha3\beta4^*$ nAChR is consistent with the observation that 7.25 μM DHβE does not block the $\tau4$ component, given that human $\alpha3\beta4$ nAChR expressed in oocytes has a K_b, the equilibrium dissociation constant for the antagonist-receptor complex, of 13.77 μM (Chavez-Noriega *et al.* 1997). High MLA concentrations, severalfold greater than the IC_{50} values, reduce access time of exogenous antagonists to the cleft and have enabled the block of putative $\alpha7^*$ and $\alpha3\beta2^*$ components within 30 to 60 min. As such, the other $\beta4$-containing candidates, $\alpha2\beta4$ and $\alpha4\beta4$, are less likely matches, as their K_b values for DHβE are 3.61 and 0.01 μM, respectively (Chavez-Noriega *et al.* 1997). Taken together these results are consistent with $\alpha3\beta4^*$ nAChRs giving rise to the $\tau4$ component.

As already noted, EPSPs associated with only a $\tau4$ component have been observed and designated as class 3 EPSPs (Table 1). While they have been observed only four times, pharmacological and kinetic dissection of composite EPSPs allows us to infer the involvement of the $\tau4$ component at another 34% of the connections studied, i.e. class 2, 5 and 6 connections (Table 1).

Relative weights of $\tau2$ and $\tau4$

An inspection of Table 1 reveals that the $\tau2$ and $\tau4$ time constants are similar and are the slowest time constants associated with the M-axon–CRN connection. The only distinct mode of the decay time constant distribution (Fig. 2) is associated with EPSPs that decay biexponentially with time constants, $\tau1$ and $\tau2$, with relative weights of 87.9 ± 4.3 and 12.1 ± 4.3%, respectively, ($n=75$). Our antagonist data indicate that the kinetic and relative weight profiles of these EPSPs, which have been assigned to class 1, are associated with $\alpha7^*$ nAChRs. For the case in which the long decay time constant is not associated with the fastest decay time constant, $\tau1$, it is designated as $\tau4$ and not $\tau2$. Antagonist data suggest that $\alpha3\beta4^*$ nAChRs produce the $\tau4$ kinetic profile of class 3 EPSPs. The designation of $\tau2$ and $\tau4$ is straightforward in each of these cases. However, the situation is more complex if $\tau1$, $\tau2$ and $\tau4$ are all present at a given connection. Two EPSP classes

Figure 4. Pharmacological dissection of class 2 and class 3 EPSPs

For *A–C*, superimposed records of averaged class 2 EPSPs in control (black) and after perfusion with antagonist for $\sim$30 min (green) and the difference trace (blue). Control is fitted (offset thin black line) with the sum of two exponentials, $\tau3$ and $\tau4$. Monoexponential fits of the decays for the difference ($\tau3$) and antagonist-insensitive ($\tau4$) peaks are marked with offset thin black lines. *A*, 1.5 μM MLA, Control: $\tau3 = 4.9$ and $\tau4 = 12.8$ ms, Difference: $\tau3 = 4.5$ ms, Antagonist insensitive: $\tau4 = 13.5$ ms. *B*, 2 μM DHβE, Control: $\tau3 = 7.5$ and $\tau4 = 11.3$ ms, Difference: $\tau3 = 7.5$ ms, Antagonist insensitive: $\tau4 = 13.2$ ms. *C*, 200 nM α-Ctx GIC, Control: $\tau3 = 6.4$ and $\tau4 = 16.7$ ms, Difference: $\tau3 = 6.7$ ms, Antagonist insensitive: $\tau4 = 20.2$ ms. *D*, superimposed records of averaged of class 3 EPSP in control (black), after perfusion with 10 μM α-Ctx AuIB $\sim$30 min (green) and after washing out the antagonist for $\sim$15 min (grey). Control: $\tau4 = 14.4$ ms, Mostly blocked: $\tau4 = 20.8$ ms, after wash: $\tau4 = 24.9$ ms.
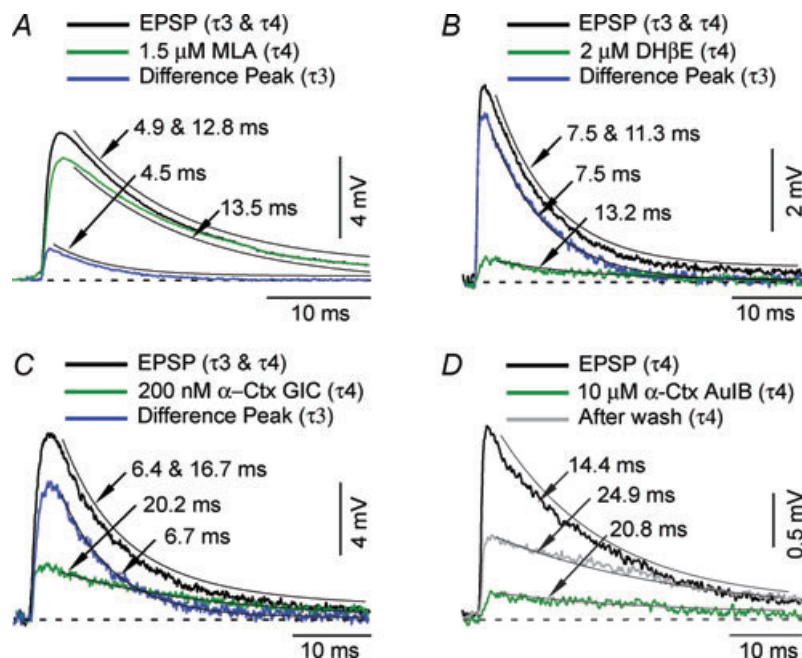
contain these decay time constants, class 5 ($\tau1$, $\tau2$ and $\tau4$) and class 6 ($\tau1$, $\tau2$, $\tau3$ and $\tau4$) (Table 1). In some cases, kinetic analysis yields different values for $\tau2$ and $\tau4$, which are determined to not be redundant by use of the *F* test. In these analyses $\tau2$, associated with the $\alpha7^*$ nAChRs, and $\tau4$, associated with $\alpha3\beta4^*$ nAChRs, are readily assigned. The long decay time constant that most closely matches the $\tau1/\tau2$ relative weight ratio for class 1 EPSPs as indicated in Table 1 is given the designation $\tau2$ and the other long decay time constant is designated as $\tau4$.
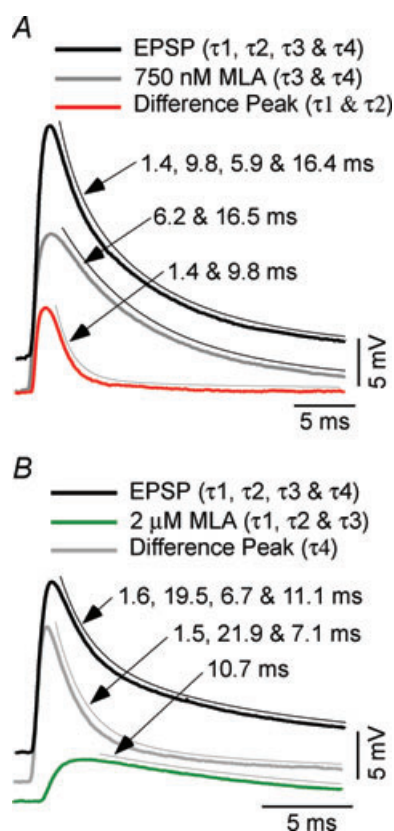

Figure 5. Curve fit of class 6 EPSPs and effect of two concentrations of MLA

A, EPSP of class 6 CRN (thick black) is fitted as the sum of four decay exponentials $\tau1 = 1.4$, $\tau2 = 9.8$ ms, $\tau3 = 5.9$ ms and $\tau4 = 16.4$ ms with weights of 7.8, 1.0, 12.3 and 5.3 mV, respectively. The EPSP is partially blocked by 750 nM MLA, leaving a response (grey) fitted by two exponentials, $\tau3 = 6.2$ and $\tau4 = 16.5$ ms with weights of 11.7 and 5.0 mV, respectively. The difference trace (red), representing the component blocked by MLA, is fitted with a double exponential, $\tau1 = 1.4$ and $\tau2 = 9.8$ ms with relative weights of 7.9 and 1.0 mV. *B*, EPSP of class 6 CRN (thick black) is fitted as the sum of four decay exponentials $\tau1 = 1.6$, $\tau2 = 19.5$ ms, $\tau3 = 6.7$ ms and $\tau4 = 11.1$ ms with weights of 11.4, 2.6, 2.2 and 4.6 mV, respectively. The EPSP is partially blocked by 2 μM MLA, leaving an antagonist-insensitive component (green), fitted by a single exponential, $\tau4 = 10.7$ ms with a weight of 4.5 mV. The difference trace (grey) is fitted by three exponentials, $\tau1 = 1.5$, $\tau2 = 21.9$ and $\tau3 = 7.1$ ms with weights of 11.9, 2.3 and 2.1 mV, respectively, representing the components blocked by MLA. Stimulus and calibration artifacts are removed from the tail of each class 6 EPSP to facilitate curve fitting. All fits (thin black lines) are offset for clarity.

However, if $\tau2$ and $\tau4$ have values such that a kinetic analysis only assigned one value to the slowly decaying phase (>8 ms), $\tau2/\tau4$, we apportioned the weight of this slowly decaying phase between $\tau2$ and $\tau4$. In order to estimate the relative contribution of $\tau2$- and $\tau4$-associated nAChRs to a composite EPSP, we used the observation that class 1 EPSPs, believed to be mediated by $\alpha7^*$ nAChRs have a ratio of weights, $\tau2_w/\tau1_w$, of 0.124 (Table 1, first 48 class 1 EPSPs). The weight of the $\tau4$ component, $W\tau4$, can be estimated from the combined weight of $\tau2$ and $\tau4$ ($W\tau2/\tau4$) using the formula:

$$W\tau4 = W\tau2/\tau4 - (W\tau1 * \tau2_w/\tau1_w),$$

where $W\tau1$ is the weight of the $\tau1$ component.

Combination of fast with intermediate and/or slow decay: EPSP classes 4–6

Kinetic analysis suggests that additional receptor combinations mediate a significant fraction of the EPSPs, namely class 4 ($\alpha7^*$ and $\alpha3\beta2^*$) and class 5 ($\alpha7^*$ and $\alpha3\beta4^*$), and class 6, which not only contains all kinetic components ($\alpha7^*$, $\alpha3\beta2^*$ and $\alpha3\beta4^*$), but has also been investigated with antagonists and is described below.

Three populations of receptors have been identified so far. Class 1 EPSPs with two decay time constants, $\tau1$ and $\tau2$, have been attributed to only one receptor type, the $\alpha7^*$ nAChR. Class 2 EPSPs have decay time constants of $\tau3$ and $\tau4$ and are most probably mediated by $\alpha3\beta2^*$ and $\alpha3\beta4^*$ nAChRs, respectively. Kinetic analysis indicates that class 6 responses (Fig. 5*A* and *B*) exhibit $\tau1/\tau2$, $\tau3$ and $\tau4$ components, suggesting that EPSPs of this class are mediated by a combination of three different nAChRs, $\alpha7^*$, $\alpha3\beta2^*$ and $\alpha3\beta4^*$. In the first illustrated example (Fig. 5*A*), the control EPSP decay was fitted as the sum of four exponentials, $\tau1 = 1.4$ ms, $\tau2 = 9.8$ ms, $\tau3 = 5.9$ ms and $\tau4 = 16.4$ ms. The $\alpha7^*$ EPSP component, blocked by 750 nM MLA and illustrated as a difference peak, has a decay phase best fitted by two exponentials, $\tau1 = 1.4$ and $\tau2 = 9.8$ ms, consistent with the presence of $\alpha7^*$ nAChRs. The EPSP components that were insensitive to 750 nM MLA in this experiment were fitted by two exponentials, $\tau3 = 6.2$ and $\tau4 = 16.5$ ms. These values for $\tau3$ and $\tau4$ are consistent with the presence of $\alpha3\beta2^*$ and $\alpha3\beta4^*$ nAChRs, respectively. Since 200 nM MLA can block $\alpha6\beta2^*$ nAChRs in rat (Mogg *et al.* 2002), the contribution of $\alpha6\beta2^*$ nAChRs has yet to be ruled out in class 6 EPSPs.

The multiexponential fit of the decay in the second illustrated class 6 EPSP example (Fig. 5*B*) has four decay times, with $\tau1$–$\tau4$, being 1.6, 19.5, 6.7 and 11.1 ms, respectively. In this case we found that 2 μM MLA blocked the $\tau1$, $\tau2$ and $\tau3$ components and isolated the $\tau4$ EPSP component with a decay time of 10.7 ms. The fit of the decay of the MLA-sensitive EPSP components yielded

values of $\tau 1$, $\tau 2$ and $\tau 3$ equal to 1.5, 21.9 and 7.1 ms, respectively. Thus, the values of $\tau 1$–$\tau 4$ derived from the fit of the decay of the control EPSP correspond quite well to the estimates obtained separately from analysis of MLA-sensitive and -insensitive EPSPs components. Based on these kinetic profiles and the MLA sensitivities of goldfish nAChRs established in this study, we suggest that these results indicate $\alpha 7^*$ and $\alpha 3\beta 2^*$ nAChRs were blocked by 2 μM MLA and that only an $\alpha 3\beta 4^*$ nAChR-mediated response remained. Table 1 provides the decay time constants and weights of the components comprising the six classes we have identified. The time constants as blocked or isolated by antagonists are: $\tau 1 = 1.6 \pm 0.2$, $n = 9$, $\tau 2 = 13.4 \pm 8.0$, $n = 9$, $\tau 3 = 6.0 \pm 1.7$ ms, $n = 4$, $\tau 4 = 13.2 \pm 3.8$ ms, $n = 6$. Although transmission was mediated by $\alpha 7^*$ nAChRs alone at the majority of the connections studied, multiple nAChR types mediated transmission at a large fraction of connections.

In both class 6 cases the absolute weight of the residual components, noted in the figure legend (Fig. 5A–B), matches the weight of those components determined by analysis of the decay kinetics of the unblocked EPSP. This suggests that the nAChRs are located only postsynaptically. A presynaptic locus might alter release probability and the weight of the components between the control and antagonized conditions.

Decay kinetics of mEPSPs

The M-axon–CRN parallel branch connection comprises a few contacts with multiple active zones (Hackett *et al.*

1989) and as indicated gives rise to the majority of these multiple exponential EPSPs. This raises several questions about the structure of the connection. Is the transmitter released at a contact detected by only one or by several receptor types? If several receptor types mediate the signal at one contact, are distinct receptor types or a mixture of receptor types associated with each postsynaptic density (PSD) in apposition to an active zone?

We postulated that aspects of the arrangement of the nAChRs at the M-axon–CRN connection could be inferred from the kinetics of the mEPSPs if the sampled mEPSPs were due to asynchronous release from only one M-axon. While there are multiple soma–dendritic inputs to the hatchetfish giant-fibre cell body, a CRN analogue (Barry & Bennett, 1990), the only known axonal inputs are from the two M-axons. Thus, we took advantage of this fact by injecting a steady subthreshold depolarizing current directly into one M-axon, so that the frequency of mEPSPs attributed to that M-axon could be enhanced.

Most often no mEPSP activity was observed in the absence of current injection. When observed, the basal frequency of mEPSPs averaged 1.8 ± 1.3 events s^{-1} ($n = 6$) (Fig. 6A). The mEPSP frequency increased dramatically as the depolarizing current in the M-axon was increased from 0 to 20 nA. Figure 6A is an example from a connection characterized as having a class 1 EPSP. A comparison of the number of mEPSP events recorded in the presence or absence of depolarizing current is illustrated in the amplitude histogram of Fig. 6B, and it shows that the depolarized M-axon is the main source of the mEPSPs. The events ratio (depolarized to control) in Fig. 6B is 12.2 and
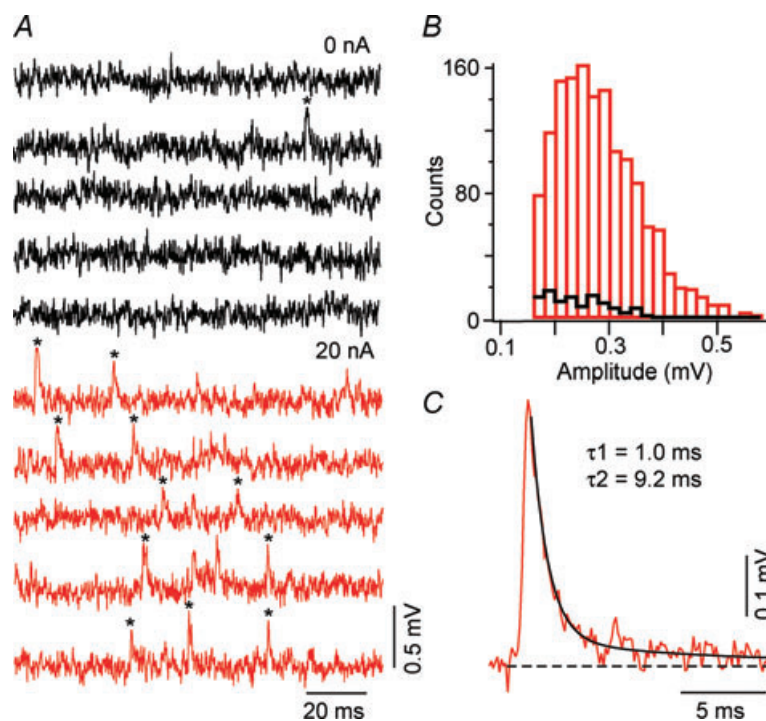

Figure 6. M-axon is the main source of mEPSPs in CRN axons
A, black and red traces are continuous recordings from a class 1 CRN with 0 nA (black) and 20 nA (red) depolarizing current injected steadily into the presynaptic M-axon. mEPSPs that meet criteria for use in averages are marked with an asterisk. *B*, amplitude histogram for mEPSPs recorded at 0 nA (black) and 20 nA (red) M-axon depolarization. *C*, averaged mEPSP of class 1 CRN is fitted by two exponentials, $\tau 1 = 1.0$ ms and $\tau 2 = 9.2$ ms.

overall was 10.2 ± 5.4 ($n = 6$). The decay time constants of an averaged mEPSP for this connection (Fig. 6C), $\tau1 = 1.0$ ms and $\tau2 = 9.2$ ms, coincide with those of the class 1 EPSPs (Table 1).

Different nAChRs distributed in separated clusters

We next asked if the waveforms of mEPSPs could allow us to determine whether receptor populations were isolated or mixed at connections with composite EPSPs. For example, the presence of two populations of mEPSPs that decayed with different time constants, $\tau3$ and $\tau4$, at a class 2 connection, putatively associated with $\alpha3\beta2^*$ and $\alpha3\beta4^*$ nAChRs, would imply separate receptor clusters. However, detection of only one mEPSP population with a biexponential decay, $\tau3$ and $\tau4$, would imply that $\alpha3\beta2^*$ and $\alpha3\beta4^*$ nAChRs were intermingled within a receptor cluster (Sargent, 2009). We approached this problem by constructing mEPSP decay time distributions, averaging mEPSPs taken from each mode of the distribution and analyzing decay kinetics of these averaged mEPSPs.

By depolarizing one M-axon, populations of mEPSPs were collected from connections at which the EPSPs were of class 1, 2 or 6. When the evoked responses were mediated by only one nAChR, as with connections mediated by class 1 EPSPs, the decay time distributions of the associated mEPSPs were uni-modal. This is depicted in Fig. 7A, where the mean decay time constant was 1.2 ms. In this particular case, a sufficient number of these mEPSPs were averaged to adequately improve the signal-to-noise ratio and the second slower exponential associated with $\alpha7^*$ nAChR EPSP decay, $\tau2$, emerged (Fig. 7A, right). That is, this averaged class 1 mEPSP could be fitted by two exponentials, $\tau1 = 1.0$ and $\tau2 = 10.1$ ms. The weight of the second exponential was 13.8% of the total amplitude, consistent with the weighting for the evoked signal being $12.1 \pm 4.3\%$ ($n = 75$). Overall, including those cases in which only $\tau1$ was resolved, the mEPSP decay associated with class 1 EPSPs was $\tau1 = 1.1 \pm 0.4$, $n = 6$.

At class 2 and class 6 connections, at which evoked responses were composites, mEPSP decay time distributions were bi-modal (Fig. 7B) or tri-modal (Fig. 7C), respectively. These distributions were also obtained by treating single events as having monoexponential decays. Therefore, additional decay time constants may have been missed at this point in the analysis. To test for composite mEPSPs and improve the signal-to-noise ratio, responses in each mode of a distribution were averaged. As shown in Fig. 7B and C, these averaged mEPSPs all decayed monoexponentially, indicating that in class 2 and class 6 EPSPs the different nAChR subtypes mediating these responses were in separate clusters. Additionally, averaged mEPSP decay time constants of the class 2 connection ($\tau3 = 5.2 \pm 0.4$,

$\tau4 = 10.3 \pm 1.5$, $n = 3$) were consistent with the taus attributed to the $\alpha3\beta2^*$ and $\alpha3\beta4^*$ nAChR-mediated EPSPs and those obtained for a class 6 connection ($\tau1 = 0.6 \pm 0.3$, $\tau3 = 5.8 \pm 0.9$, $\tau4 = 10.6 \pm 2.0$, $n = 3$, $P < 0.05$ for $\tau1$ *vs.* $\tau3$ or $\tau4$ and for $\tau3$ *vs.* $\tau4$) were consistent with those attributed to the $\alpha7^*$, $\alpha3\beta2^*$ and $\alpha3\beta4^*$ nAChR-mediated EPSPs. Note that at the class 6 connection of Fig. 7C the signal-to-noise ratio of the averaged $\alpha7^*$ mEPSPs was such that the slow decay time constant could not be extracted from the noise. Therefore only the fast time constant is indicated. The lack of mEPSPs fitted by multiple exponentials associated with different nAChR types is in contrast to those seen in chick ciliary ganglion neurons (Chen *et al.* 2001; Sargent, 2009).

To confirm the validity of averaging minis by their rising edge, the class 6 mini data were also aligned by their peaks for averaging and the decays of the averaged mEPSPs were subsequently fitted with one and two exponentials. In all cases, these averaged minis were again best fitted by one exponential as per *F* test criteria. Additionally, at one class 6 connection where the M-axon-CRN pair was held long enough to observe the influence of 100 nM MLA, $\tau1$ ($n = 13$) and $\tau3$ ($n = 10$) asynchronous minis before the block reduced to only $\tau3$ ($n = 7$) minis after the block (data not shown).

Up to three contact sites were detected between the parallel branch of the CRN and the M-axon (Fig. 8A), and these were separated by more than 50 μm. In contrast, only one contact was ever observed on the crossing branch of the CRN. The finding that mEPSPs are not composite, but rather are generated by activation of homogeneous receptor populations, implies that the different receptor types are functionally isolated from each other. This functional organization could be achieved in two ways: either each of several contacts between a M-axon and a CRN involves a single receptor type, or the different receptors are segregated into separate clusters within a contact having multiple active zones (Hackett *et al.* 1989). The latter is the likely structure for the contralateral M-axon–CRN connection where only one contact has been observed and would require sufficient separation between neighbouring active zones, and their apposed postsynaptic sites, to preclude activation by spillover with low-frequency activation (Hartzell *et al.* 1975; Faber *et al.* 1985; Faber & Korn, 1988).

Overall, we observed M-axon collateral structures that would allow for the separation of receptor clusters (e.g. Fig. 8B). In these experiments, receptors located at these sites were identified with α-Btx. An example from a different experiment of a contact site between an M-axon and a crossing CRN axon that exhibited class 1 EPSPs is shown in Fig. 8C. In this case, the EPSP was mediated by $\alpha7^*$ nAChRs only. In another experiment, an $\alpha7^*$ nAChR contact of an ipsilateral M-axon–CRN connection exhibiting class 1 EPSPs was found ~200 μm rostral

to the intersection of the contralateral M-axon and the crossing branch of the CRN (Fig. 8*Da*). An enlarged three-dimensional rendering of this contact site (Fig. 8*Db*) shows the $\alpha 7^*$ nAChR embedded in the postsynaptic CRN axon. The nAChRs appear to be embedded in the CRN terminal and not associated with the M-axon, consistent with what we observed as we stepped through the confocal stacks of such connections. Additionally, transmission electron microscopy studies showed a postsynaptic locus for α-Btx staining of receptors at the homologous connection in the hatchetfish (Day *et al.* 1983).

Discussion

The major findings of this study are that (1) multiple subtypes of nAChRs can mediate the EPSPs at the connection between an M-axon and a CRN, with correspondingly distinct kinetics and (2) when different nAChRs are present they appear to be segregated into separate clusters. These conclusions are based upon comparison of the kinetic properties of spike-triggered EPSPs with those of mEPSPs attributed to release of single quanta, as well as the pharmacological profiles of the EPSPs. Through the use of antagonists we identified three pharmacologically

Figure 7. CRN mEPSPs are not composites

A, B and *C*, comparison of decay kinetics of evoked and mEPSPs, for class 1, class 2 and class 6 connections, respectively. In each example, averaged evoked EPSPs (left panel, *A* and upper left panels, *B* and *C*) have multiple exponential decays as indicated by τ values. The corresponding mEPSP decay time histograms (centre, *A* and lower left panels, *B* and *C*) are fitted as the sums of one, two or three Gaussians, respectively. In right panel, *A*, and lower right panels, *B* and *C*, are averaged mEPSPs for traces selected from each mode. In the upper right panels, *B* and *C*, are continuous recordings with mEPSPs of varying decay kinetics. *A*, class 1 EPSP decay is fitted by two exponentials, with $\tau 1 = 1.3$ and $\tau 2 = 10.6$ ms. The histogram of mEPSP decay times is fitted as one Gaussian. The decay times of the corresponding averaged mEPSP are $\tau 1 = 1.0$ and $\tau 2 = 10.1$ ms. *B*, class 2 EPSP decay is fitted with two exponentials $\tau 3 = 5.0$ and $\tau 4 = 15.9$ ms. The histogram of mEPSP decay times is fitted as the sum of two Gaussians. The decay times of the corresponding averaged mEPSPs are $\tau 3 = 4.9$ and $\tau 4 = 9.3$ ms. *C*, class 6 EPSP decay is fitted by three exponentials $\tau 1 = 1.2$, $\tau 3 = 7.4$ and $\tau 2/\tau 4 = 11.7$ ms. The histogram of mEPSP decay times is fitted as the sum of three Gaussians. The decay times of the corresponding averaged mEPSPs are $\tau 1 = 0.5$, $\tau 3 = 4.9$ and $\tau 4 = 9.1$ ms.
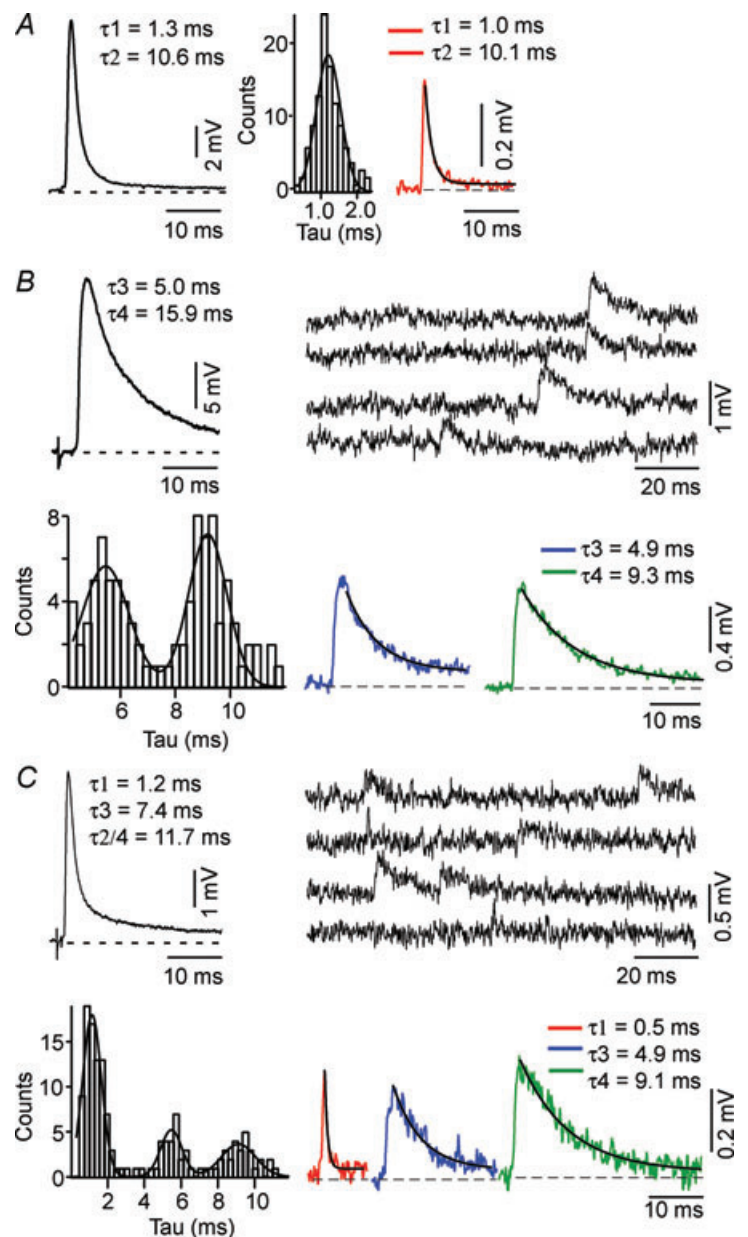
distinguishable nAChR populations associated with the EPSPs. Population 1 nAChRs, putatively $\alpha 7^*$, were sensitive to MLA, α-Btx and α-Ctx ArIB[V11L;V16D], population 2 nAChRs, putatively $\alpha 3\beta 2^*$, were sensitive to MLA, DHβE, α-Ctx GIC and population 3 nAChRs, putatively $\alpha 3\beta 4^*$, were sensitive to α-Ctx AuIB.

Filtering

The morphological relationships described here support the argument that EPSPs and mEPSPs recorded in a CRN accurately reflect the decay kinetics of the nAChRs and are not subject to significant filtering by axonal cable properties, even in the case of the fast $\alpha 7^*$ nAChR responses (Jack *et al.* 1975). The CRN axon, which is myelinated, had a membrane time constant of $\sim 400\,\mu$s and a length constant, λ, of ~ 2 mm (Funch *et al.* 1984), based on paired recordings from the same axon in two experiments. This decay time constant was less than that of any of the EPSP components. Thus, unless the CRN electrode was electrotonically quite far from the synaptic loci, which would be inconsistent with the morphology, the measured decay kinetics accurately reflect the time course of deactivation for putative $\alpha 3\beta 2^*$ and $\alpha 3\beta 4^*$ nAChR channels. The $\tau 1$ component kinetics ($\alpha 7^*$ nAChRs) of ~ 1.7 ms may be degraded, but only moderately.

Based on the contact locations observed with confocal microscopy, the maximum distance between the CRN recording site and the contact would be 400–500 μm, or
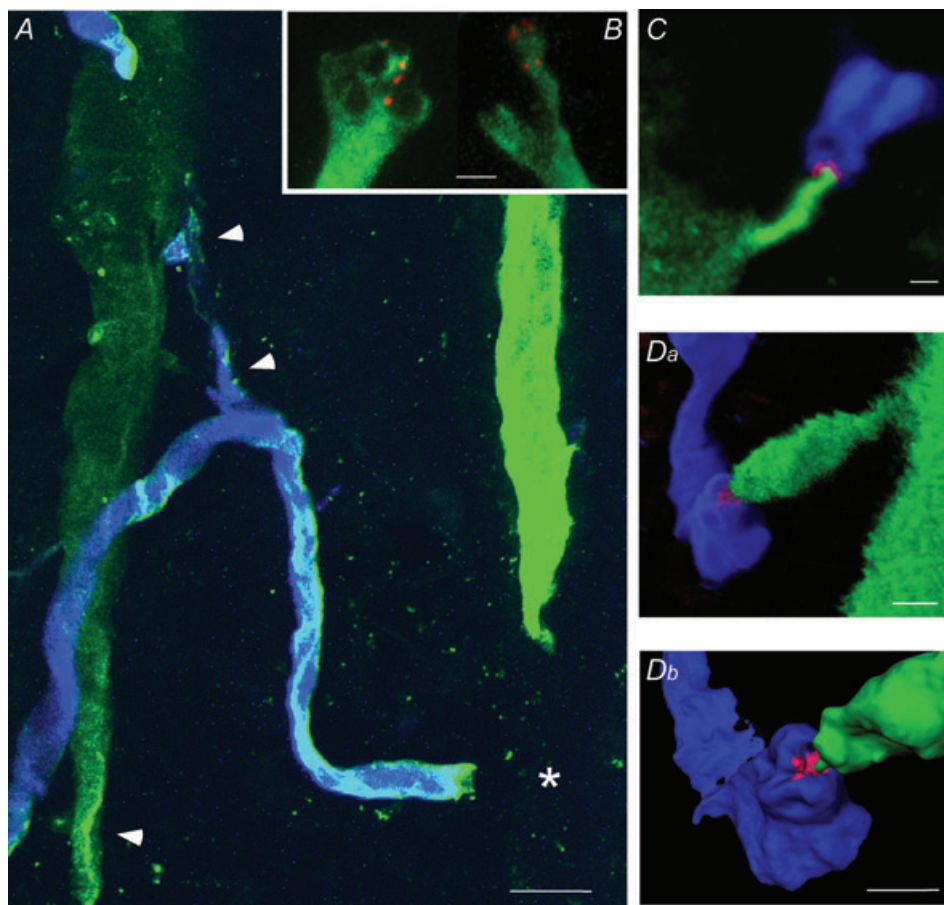

Figure 8. M-axon and CRN anatomy and contact sites
A, *B*, *C* and *D* are confocal images from four separate preparations depicting the M-axon (green), CRN (blue) and $\alpha 7^*$ nAChRs (red). *A*, three putative contact locations, marked by arrowheads, between the ipsilateral M-axon and CRN. The approximate location of the contact site between the CRN and contralateral M-axon (not captured in this slice), is marked by an asterisk (*). Calibration bar equals 50 μm. *B*, two examples of M-axon collaterals exhibiting structures that could support the segregation of different nAChR types. *C*, high magnification of the contact associated with the crossing branch of a CRN with class 1 EPSPs (location in *A*, but different preparation). Overlap of CRN (blue) and $\alpha 7^*$ nAChRs (red) depicted by rose colour. *Da*, Z-stack image of a contact associated with the parallel branch of the CRN (location near rostral contact and arrowhead in *A*, but different preparation). *Db*, a thresholded rendering of same contact seen in *Da* magnified and tilted to highlight $\alpha 7^*$ nAChRs and CRN structure. *B–D*, calibration bars equal 5 μm.

$\sim$0.25λ. In confirmation, we measured the decrement and filtering of two types of responses recorded simultaneously with two electrodes that were in the same CRN axon and separated by 350 to 500 μm: (i) an EPSP evoked by caudal spinal cord stimulation, was reduced in amplitude by about 20% rostrally, but its kinetics were unchanged, and (ii) the full width half maximum of a passively conducted action potential evoked by current injected caudally increased only slightly, from 1.1 to 1.2 ms. The action potential propagated passively because QX-314 diffusing from the rostral electrode blocked voltage-dependent sodium current locally. Finally, the frequency of minis with intermediate, $\sim$5 ms, and long, $\sim$10 ms, decay time constants did not change after treatment with 200 nM MLA to block $\alpha7^*$ nAChR receptors, while those with the fast decay time constant disappeared. This observation indicates that the minis associated with tau values > 2.5 ms were not filtered $\alpha7^*$ mEPSPs generated at sites distant from the recording electrode.

Specificity of pharmacological dissection

The pharmacological profile for $\alpha7$, $\alpha3\beta2$ and $\alpha3\beta4$ nAChRs in the goldfish may be different to that for other species. Much of the pharmacology for these receptors has been studied in oocyte expression systems and in rat, mouse and chick. BLAST and VAST analyses were used to find the common structural and sequence features between the teleost (goldfish and/or zebrafish) and the species in which the specificity of antagonists had been demonstrated. Comparison of sequence and structural homology across species with each of the $\alpha7$, $\alpha3$, $\beta2$ and $\beta4$ nAChR subunit goldfish or zebrafish gene sequences shows a high degree of identity. This holds true particularly in the case of the sequence fragments and residues of $\alpha7$, $\alpha3$ and $\beta2$ nAChR subunits known to be critical for binding the pertinent ligands used in this study.

Due to potential species differences, we cannot definitively assign specific receptor subtypes to a population type. Nevertheless, the nAChR populations in the goldfish M-axon–CRN connection are consistent with $\alpha7^*$ (population 1), $\alpha3\beta2^*$ (population 2) and $\alpha3\beta4^*$ (population 3) by analogy to mammalian and chick nAChRs. These three populations contribute to six classes of EPSPs that have different decay time constants as follows: class 1 ($\tau1$, $\tau2$, population 1 nAChRs), class 2 ($\tau3$, $\tau4$, populations 2 and 3 nAChRs), class 3 ($\tau4$, population 3 nAChRs), class 4 ($\tau1$, $\tau2$, $\tau3$, populations 1 and 2 nAChRs), class 5 ($\tau1$, $\tau2$, $\tau4$, populations 1 and 3 nAChRs) and class 6 ($\tau1$, $\tau2$, $\tau3$, $\tau4$, populations 1, 2 and 3 nAChRs). The pharmacological sensitivities of the different EPSP components and their kinetics are consistent with known properties of the different nAChRs in other species.

Class 1 EPSPs are completely blocked by 35–50 nM MLA. For comparison, $\alpha7$ nAChRs in rat dorsal root ganglion neurons (Genzen *et al.* 2001), rat dorsal motor vagal neurons (Sahibzada *et al.* 2002), rat striatal slices (Kaiser & Wonnacott, 2000) and rat superior cervical ganglion neurons (Cuevas *et al.* 2000) were blocked by 10 nM, 10 nM, 50 nM and 200 nM MLA, respectively. Class 1 EPSPs were also blocked by 50–100 nM α-Btx, the concentrations typically used to block putative $\alpha7^*$ nAChRs (Day *et al.* 1983; Zhang *et al.* 1996; Ullian *et al.* 1997; Chang & Berg, 1999; Sahibzada *et al.* 2002). At the M-axon–CRN connection, the α-Btx and MLA blocks were not reversible after up to 45 min of washing. A block of putative $\alpha7^*$ nAChRs with 50 nM α-Btx was similarly found to be irreversible in chick ciliary ganglion (Ullian *et al.* 1997).

Both α-Btx and MLA block $\alpha9^*$ nAChRs (Elgoyhen *et al.* 2001; Baker *et al.* 2004) and α-Btx also blocks $\alpha1^*$ nAChRs. MLA also blocks $\alpha6\beta2^*$ nAChRs (K_i 33 nM), (Mogg *et al.* 2002). Therefore, to further establish that goldfish class 1 EPSPs are probably mediated by $\alpha7^*$ nAChRs we utilized 150 nM α-Ctx ArIB to block a class 1 EPSP (Fig. 3*D*). α-Ctx ArIB is a new $\alpha7$ nAChR antagonist that does not block $\alpha1^*$, $\alpha2^*$, $\alpha3^*$, $\alpha4^*$, $\alpha6^*$ or $\alpha9^*$ nAChRs (Whiteaker *et al.* 2007).

The pharmacological profiles of $\alpha7^*$ nAChRs in the goldfish may be different to those in mammalian and avian homologues and require longer access times, particularly in an *in vivo* preparation. However, comparison across species of sequence and structural homology of the $\alpha7$ nAChR ligand binding domain (Brejc *et al.* 2001) with that of the zebrafish, indicates a high level of identity with human, rat, mouse and chick (Table 2). The zebrafish and goldfish are both members of the teleost infraclass and are expected to have similar antagonist sensitivities. Indeed, they show 100% sequence identity in the nAChR binding domain.

MLA binding to the acetylcholine binding protein, a surrogate for the nAChR binding domain, includes interactions with 14 residues of the $\alpha7$ nAChR subunit interfaces, four of which are specific to MLA (Hansen *et al.* 2005). At these 14 interaction sites, the zebrafish subunits share 100% and 78.6% identity with residues of chick and mammalian subunits, respectively (Supplemental Fig. S1). Overall, in the ligand binding domain, the zebrafish shares 82.5–83% gene sequence identity with chick, rat, mouse and human (Table 2). These homologies suggest that zebrafish and goldfish $\alpha7$ nAChRs have similar MLA sensitivities to those of human, rat and mouse, but particularly chick.

Only one decay time constant has been associated with putative $\alpha7$ nAChR responses to synaptic current in the chick ciliary ganglion preparation, 1.84 ± 0.14 ms (Zhang *et al.* 1996) and 1.04 ± 0.35 ms (Ullian *et al.* 1997), and our observed $\tau1$ value of class 1 EPSPs is in good agreement with these reports. However, two decay time constants

Table 2. Percentage sequence identity

	Binding domain $\alpha 7$ Zebrafish	14 Antagonist interaction sites $\alpha 7$ Zebrafish	4 MLA specific sites $\alpha 7$ Zebrafish	Binding domain $\alpha 3$ Goldfish	Binding domain $\beta 2$ Goldfish	Binding domain $\beta 4$ Goldfish
Human	83.0	78.6	50	79.8	77.8	75.6
Rat	82.5	78.6	50	77.9	77.3	74.6
Mouse	82.5	78.6	50	77.9	77.3	74.6
Chick	82.5	100	100	78.4	78.4	79.9
Zebrafish	100	100	100	99.0	96.4	100
Pufferfish	___	___	___	___	___	91.4

Cysteines: $\alpha 7$ at 190, 191 (Hansen *et al.* 2005); $\alpha 3$ at 192, 193 (Cauley *et al.* 1990; Hieber *et al.* 1990a); $\beta 2$ at 130, 144 (Heiber *et al.* 1990b); $\beta 4$ at 130, 144 (XP 696993, NCBI database).

have been reported for $\alpha 7$ nAChR-mediated synaptic current in hippocampal interneurons in rat brain slices (Frazier *et al.* 1998). In our study the nAChRs that underlie the two time constants, $\tau 1$ and $\tau 2$, of class 1 EPSPs are both sensitive to $\alpha 7$ nAChR antagonists. In that kinetic elements of class 1 EPSPs do not exhibit a differential sensitivity to antagonists (Fig. 3*Ca* and *b*), it is unlikely that two different receptor types give rise to $\tau 1$ and $\tau 2$ (Frazier *et al.* 1998).

Three possible explanations for the source of the second kinetic element, $\tau 2$, are (1) the lack of desensitization of homomeric $\alpha 7$ nAChRs, (2) the presence of heteromeric $\alpha 7^*$ nAChRs and (3) a small contribution from $\alpha 3 \beta 4^*$ nAChRs not detected by kinetic analysis. The biexponential decay of class 1 EPSPs could reflect multiple open states or burst properties (Nai *et al.* 2003) and the absence of desensitization at agonist concentrations and profiles generated in the synaptic context, enabling the presence of a slowly decaying current similar to the $\tau 2$ element, (Frazier *et al.* 1998; Papke & Thinschmidt, 1998; Papke *et al.* 2000; Mike *et al.* 2000; Shoop *et al.* 2001; Placzek *et al.* 2005). In a few cases $\alpha 7$ nAChRs have been reported to occur as a heteromers in association with $\beta 2$ subunits (Yu & Role, 1998; Shao & Yakel, 2000). It is possible that in our preparation a similar situation might account for the two observed time constants. Lastly, a small contribution from $\alpha 3 \beta 4^*$ nAChRs may be misidentified as a $\tau 2$ element in class 1 EPSPs analysed only by decay kinetics, but this cannot account for the susceptibility of the $\tau 2$ element to antagonists specific for $\alpha 7$ nAChRs.

The $\tau 3$ component is blocked by an $\alpha 3 \beta 2$ nAChR-specific antagonist, α-Ctx GIC (McIntosh *et al.* 2002), and has decay kinetics similar to synaptically evoked monoexponential EPSCs ($\sim$5–7 ms) (Ullian *et al.* 1997; Chen *et al.* 2001) in the chick ciliary ganglion. The ciliary $\alpha 3^*$ EPSCs are mediated in part by $\alpha 3$ and $\beta 2$ subunits (Conroy & Berg, 1995), are blocked by α-Ctx MII (Ullian *et al.* 1997; Chen *et al.* 2001), an antagonist that targets

$\alpha 3 / \beta 2$ nAChRs interfaces (Cartier *et al.* 1996), and are associated with a 40 pS nAChR channel having a mean open time of $\sim$2.8 ms under 0.5 μM nicotine activation (Nai *et al.* 2003).

Comparison of sequence homology across species within the nAChR ligand binding domain (Brejc *et al.* 2001) for the goldfish $\alpha 3$ (Cauley *et al.* 1990; Hieber *et al.* 1990a) and goldfish $\beta 2$ (Hieber *et al.* 1990b) nAChR subunit gene sequences reveals 77–80% identity, as shown in Table 2. Note that there is a very high identity, 96–99%, between goldfish and zebrafish. The sequence fragments and residues crucial for binding α-Ctx GIC, one of the antagonists used in the present pharmacological investigation of the $\tau 3$ component, are inferred by comparison with α-Ctx MII and outlined in vertical registers in Supplemental Fig. S2*A* and *B*. The goldfish $\alpha 3$ and $\beta 2$ nAChR sequences contain the same residues shown to be critical for binding α-Ctx MII in the $\alpha 3 \beta 2$ human nAChR, namely K185 and I188 for the $\alpha 3$ subunit and T59 for the $\beta 2$ subunit (Harvey *et al.* 1997; Chi *et al.* 2005). α-Ctx MII and α-Ctx GIC are expected to have similar interactions with $\alpha 3 \beta 2$ nAChRs, based on structural analysis (Chi *et al.* 2004). Additionally, the high level of sequence and structural homology across species suggest that MLA and α-Ctx GIC are likely to interact with the goldfish $\alpha 3 \beta 2$ nAChRs as they do in other species (Table 2).

The $\tau 4$ EPSP component is blocked by an $\alpha 3 \beta 4$-specific antagonist, α-Ctx AuIB (Luo *et al.* 1998). Interestingly a ciliary $\alpha 3^*$ channel lacking the $\beta 2$, but containing the $\beta 4$, subunit had a slightly longer mean open time, $\sim$3.2 ms, than its $\alpha 3 \beta 2^*$ counterpart (Nai *et al.* 2003). Also, $\alpha 3 \beta 4$ nAChRs expressed in oocytes (Boorman *et al.* 2003) have complex channel kinetics with a mean open time of 9.4 ms, consistent with the decay kinetics of the $\tau 4$ EPSP and mEPSP (Table 1).

The sequence identity of the teleost $\beta 4$ subunit when compared with that of human, rodents and chick

(Supplemental Fig. S2*C*) is ∼74–80% (Table 2). α-Ctx AuIB (10 μM) blocks $\alpha3\beta4$ nAChRs expressed in oocytes heterologously and in chick and rat endogenously (Luo *et al.* 1998; Nai *et al.* 2003; Park *et al.* 2006). The sites that convey this specificity are not yet known. Nevertheless, the zebrafish 54–63 segment in the $\beta4$ nAChR subunit that is part of the complementary face of the antagonist binding pocket (Brejc *et al.* 2001; Hansen *et al.* 2005) is similar across species, suggesting that this toxin may also have specificity in the goldfish.

Physiological relevance of multiple nAChR types

The M-axon action potential triggers an escape response, and the classic role for the CRNs or their analogues is to activate supraspinal motorneuron pools that control the opercular, ocular, jaw and pectoral fin muscles (Auerbach & Bennett, 1969; Diamond, 1971; Model *et al.* 1972; Hackett & Faber, 1983*a*; Hackett & Buchheim, 1984). During an escape, CRN activation leads to jaw closure, making the fish shape more streamlined (Barry and Bennett, 1990). Why are three different nAChR populations present at a connection that has a high safety factor and that is associated with a stereotyped behaviour, especially since the escape response is optimized by factors limiting M-cell activation to a single spike? Indeed it has been assumed that CRNs also do not fire repetitively. Nevertheless, the multiplicity of receptor types may enable a wide variety of important subcellular (Sabatini *et al.* 2001; Berg *et al.* 2006) and circuit-level adaptive properties (Korn & Faber, 2005). These include (1) increasing the safety factor of the connection; (2) temporal tuning of the CRN depolarization window to enhance spatial and temporal integration, for example, of delayed inputs to the CRN dendritic arbor from other reticulospinal neurons; (3) differential timing of the excitation of the different CRN classes; and (4) differential modulation of channel biophysical properties and activation of downstream pathways unique to each receptor type.

Augmenting the EPSP by activating multiple receptor components enables a fast rise time via $\alpha7^*$ nAChRs and an increased probability that threshold will be attained with the added contributions from the $\alpha3\beta2^*$ and $\alpha3\beta4^*$ receptors that prolong the EPSPs (Zhang *et al.* 1996). Both of these attributes would be consistent with the need to quickly and reliably relay the signal from the M-axon, initiating a startle response.

Behavioural observations suggest that in certain cases the escape may consist of two successive fast body bends. The input underlying the second bend could come from either the M-axon or its homologues known to participate in some escapes (Korn & Faber, 2005); in either case, the mixed signal CRNs (classes 2, 4, 5 or 6) would be more likely to integrate these inputs, especially asynchronous excitation from the homologues.

Second messengers (Tan *et al.* 1998; Du & Role, 2001; Fischer *et al.* 2005) interact with the intercellular region of particular nAChR subunits and can differentially alter the biophysical characteristics of the receptor. The presence of several receptor subtypes enables the cell to regulate multiple downstream processes simultaneously. Specific members of the PSD95 family of PDZ-containing proteins are associated with particular nAChR subtypes (Conroy *et al.* 2003; Baer *et al.* 2007) and mediate such processes (Parker *et al.* 2004; Berg *et al.* 2006).

Glutamatergic synapses also are characterized by the co-activation of multiple receptor types that mediate fast synaptic transmission with different kinetics, notably AMPA and NMDA receptors. Activating NMDA receptors, which have slower kinetics and a higher Ca^{2+} permeability, has been implicated in activity-dependent plasticities of synaptic transmission. While a similar arrangement might pertain for nAChRs, it is notable that the Ca^{2+}-permeable channel, $\alpha7^*$, has the fastest kinetics.

We have demonstrated the presence of six EPSP classes coupled with at least two CRNs types (Titmus & Faber, 1987; Hackett & Buchheim, 1984), indicating a significantly greater diversity in CRNs than previously appreciated in the goldfish (Kimmel *et al.* 1985; Barry & Bennett, 1990). This has raised questions as to the physiological role of this diversity. Instead of the limited stereotyped role of CRNs in the escape response, CRNs may be associated with many more behaviours. Indeed, the possibility of varied inputs to the giant fibre cell body, a CRN homologue in the hatchet fish, suggests the involvement of the giant fibre in non-Mauthner initiated C-starts (Barry & Bennett, 1990). This system lends itself to investigating pre- and postsynaptic transmission mechanisms, and given that it can be studied *in vivo*, provides a compelling model for exploring cellular correlates of a wide variety of behaviours.

References

Alkondon M & Albuquerque EX (1993). Diversity of nicotinic acetylcholine receptors in rat hippocampal neurons. I. Pharmacological and functional evidence for distinct structural subtypes. *J Pharmacol Exp Ther* **265**, 1455–1473.

Alkondon M, Pereira EFR & Albuquerque EX (1998). α-Bungartotoxin- and methyllycaconitine-sensitive nicotinic receptors mediate fast synaptic transmission in interneurons of rat hippocampal slices. *Brain Res* **810**, 257–263.

Ankri N, Legendre P, Faber DS & Korn H (1994). Automatic detection of spontaneous synaptic responses in central neurons. *J Neurosci Methods* **52**, 87–100.

Astles PC, Baker SR, Boot JR, Broad LM, Dell CP & Keenan M (2002). Recent progress in the development of subtype selective nicotinic acetylcholine receptor ligands. *Curr Drug Targets CNS Neurol Disord* **1**, 337–348.

Auerbach AA & Bennett MV (1969). Chemically mediated transmission at a giant fiber synapse in the central nervous system of a vertebrate. *J Gen Physiol* **53**, 183–210.

Baer K, Burli T, Huh KH, Wiesner A, Erb-Vogtli S, Gockeritz-Dujmovic D *et al.* (2007). PICK1 interacts with α7 neuronal nicotinic acetylcholine receptors and controls their clustering. *Mol Cell Neurosci* **35**, 339–355.

Baker ER, Zwart R, Sher E & Millar NS (2004). Pharmacological properties of α9 α10 nicotinic acetylcholine receptors revealed by heterologous expression of subunit chimeras. *Mol Pharmacol* **65**, 453–460.

Barry MA & Bennett MV (1990). Projections of giant fibers, a class of reticular interneurons, in the brain of the silver hatchetfish. *Brain Behav Evol* **36**, 391–400.

Berg DK & Conroy WG (2002). Nicotinic α7 receptors: synaptic options and downstream signaling in neurons. *J Neurobiol* **53**, 512–523.

Berg DK, Conroy WG, Liu Z & Zago WM (2006). Nicotinic signal transduction machinery. *J Mol Neurosci* **30**, 149–152.

Boorman JP, Beato M, Groot-Kormelink PJ, Broadbent SD & Sivilotti LG (2003). The effects of β3 subunit incorporation on the pharmacology and single channel properties of oocyte-expressed human α3β4 neuronal nicotinic receptors. *J Biol Chem* **278**, 44033–44040.

Bradaia A & Trousland J (2002). Fast synaptic transmission mediated by α-bungarotoxin-sensitive nicotinic acetylcholine receptors in lamina X neurones of neonatal rat spinal cord. *J Physiol* **544**, 727–739.

Brejc K, van Dijk WJ, Klaassen RV, Schuurmans M, Van Der Oost J, Smit AB & Sixma TK (2001). Crystal structure of an ACh-binding protein reveals the ligand-binding domain of nicotinic receptors. *Nature* **411**, 269–276.

Bryant DL, Free RB, Thomasy SM, Lapinsky DJ, Ismail KA, McKay SB *et al.* (2002). Structure-activity studies with ring E analogues of methyllycaconitine on bovine adrenal α3β4* nicotinic receptors. *Neurosci Res* **42**, 57–63.

Cartier GE, Yoshikami D, Gray WR, Luo S, Olivera BM & McIntosh JM (1996). A new α-conotoxin which targets α3β2 nicotinic acetylcholine receptors. *J Biol Chem* **271**, 7522–7528.

Cauley K, Agranoff BW & Goldman D (1990). Multiple nicotinic acetylcholine receptor genes are expressed in goldfish retina and tectum. *J Neurosci* **10**, 670–683.

Chang KT & Berg DK (1999). Nicotinic acetylcholine receptors containing α7 subunits are required for reliable synaptic transmission in situ. *J Neurosci* **19**, 3701–3710.

Chavez-Noriega LE, Crona JH, Washburn MS, Urrutia A, Elliott KJ & Johnson EC (1997). Pharmacological characterization of recombinant human neuronal nicotinic acetylcholine receptors h α2β2, h α2β4, h α3β2, h α3β4, h α4β2, h α4β4 and h α7 expressed in *Xenopus* oocytes. *J Pharmacol Exp Ther* **280**, 346–356.

Chen M, Pugh PC & Margiotta JF (2001). Nicotinic synapses formed between chick ciliary ganglion neurons in culture resemble those present on the neurons *in vivo*. *J Neurobiol* **47**, 265–279.

Chi SW, Kim DH, Olivera BM, McIntosh JM & Han KH (2004). Solution conformation of α-conotoxin GIC, a novel potent antagonist of α3β2 nicotinic acetylcholine receptors. *Biochem J* **380**, 347–352.

Chi SW, Lee SH, Kim DH, Kim JS, Olivera BM, McIntosh JM & Han KH (2005). Solution structure of α-conotoxin PIA, a novel antagonist of α6 subunit containing nicotinic acetylcholine receptors. *Biochem Biophys Res Commun* **338**, 1990–1997.

Coggan JS, Bartol TM, Esquenazi E, Stiles JR, Lamont S, Martone ME *et al.* (2005). Evidence for ectopic neurotransmission at a neuronal synapse. *Science* **309**, 446–451.

Conroy WG & Berg DK (1995). Neurons can maintain multiple classes of nicotinic acetylcholine receptors distinguished by different subunit compositions. *J Biol Chem* **270**, 4424–4431.

Conroy WG, Liu Z, Nai Q, Coggan JS & Berg DK (2003). PDZ-containing proteins provide a functional postsynaptic scaffold for nicotinic receptors in neurons. *Neuron* **38**, 759–771.

Couturier S, Erkman L, Valera S, Rungger D, Bertrand S, Boulter J, Ballivet M & Bertrand D (1990*b*). α5, α3, and non-α3. Three clustered avian genes encoding neuronal nicotinic acetylcholine receptor-related subunits. *J Biol Chem* **265**, 17560–17567.

Cuevas J, Roth AL & Berg DK (2000). Two distinct classes of functional 7-containing nicotinic receptor on rat superior cervical ganglion neurons. *J Physiol* **525**, 735–746.

Dani JA & Bertrand D (2007). Nicotinic acetylcholine receptors and nicotinic cholinergic mechanisms of the central nervous system. *Annu Rev Pharmacol Toxicol* **47**, 699–729.

Day JW, Hall DH, Hall LM & Bennett MV (1983). α-Bungarotoxin labeling and acetylcholinesterase localization at the Mauthner fiber giant synapse in the hatchetfish. *J Neurosci* **3**, 272–279.

Diamond J (1971). The Mauthner cell. In *Fish Physiology*, ed. Hoar WS & Randall DJ, pp. 265–346. Academic Press, New York.

Drasdo A, Caulfield M, Bertrand D, Bertrand S & Wonnacott S (1992). Methyl lycaconitine: A novel nicotinic antagonist. *Mol Cell Neurosci* **3**, 237–243.

Du C & Role LW (2001). Differential modulation of nicotinic acetylcholine receptor subtypes and synaptic transmission in chick sympathetic ganglia by PGE_2. *J Neurophysiol* **85**, 2498–2508.

Elgoyhen AB, Vetter DE, Katz E, Rothlin CV, Heinemann SF & Boulter J (2001). α10: a determinant of nicotinic cholinergic receptor function in mammalian vestibular and cochlear mechanosensory hair cells. *Proc Natl Acad Sci U S A* **98**, 3501–3506.

Faber DS, Funch PG & Korn H (1985). Evidence that receptors mediating central synaptic potentials extend beyond the postsynaptic density. *Proc Natl Acad Sci U S A* **32**, 3504–3508.

Faber DS & Korn H (1978). Electrophysiology of the Mauthner cell: basic properties, synaptic mechanisms, and associated networks. In *Neurobiology of the Mauthner Cell*, ed. Faber DS & Korn H, pp. 47–131. Raven, New York.

Faber DS & Korn H (1988) Synergism at central synapses due to lateral diffusion of transmitter. *Proc Natl Acad Sci U S A* **85**, 8708–8712.

Faria M, Oliveira L, Timoteo MA, Lobo MG & Correia-De-Sa P (2003). Blockade of neuronal facilitatory nicotinic receptors containing α3β2 subunits contribute to tetanic fade in the rat isolated diaphragm. *Synapse* **49**, 77–88.

Figl A & Cohen BN (2000). The subunit dominates the relaxation kinetics of heteromeric neuronal nicotinic receptors. *J Physiol* **524**, 685–699.

Fischer H, Liu DM, Lee A, Harries JC & Adams DJ (2005). Selective modulation of neuronal nicotinic acetylcholine receptor channel subunits by Go-protein subunits. *J Neurosci* **25**, 3571–3577.

Flores CE, Ene S & Pereda AE (2008). An immunochemical marker for goldfish Mauthner cells. *J Neurosci Methods* **175**, 64–69.

Frazier CJ, Buhler AV, Weiner JL & Dunwiddie TV (1998). Synaptic potentials mediated via α-bungarotoxin-sensitive nicotinic acetylcholine receptors in rat hippocampal interneurons. *J Neurosci* **18**, 8228–8235.

Fucile S, Matter JM, Erkman L, Ragozzino D, Barabino B, Grassi F *et al.* (1998). The neuronal α6 subunit forms functional heteromeric acetylcholine receptors in human transfected cells. *Eur J Neurosci* **10**, 172–178.

Funch PG, Wood MR & Faber DS (1984). Localization of active sites along the myelinated goldfish Mauthner axon: morphological and pharmacological evidence for saltatory conduction. *J Neurosci* **4**, 2397–2409.

Genzen JR, Van Cleve W & McGehee DS (2001). Dorsal root ganglion neurons express multiple nicotinic acetylcholine receptor subtypes. *J Neurophysiol* **86**, 1773–1782.

Gilat E, Hall DH & Bennett MV (1986). The giant fiber and pectoral fin adductor motoneuron system in the hatchetfish. *Brain Res* **365**, 96–104.

Guo JZ, Liu Y, Sorenson EM & Chiappinelli VA (2005). Synaptically released and exogenous ACh activates different nicotinic receptors to enhance evoked glutamatergic transmission in the lateral geniculate nucleus. *J Neurophysiol* **94**, 2549–2560.

Hackett JT & Buchheim A (1984). Ultrastructural correlates of electrical-chemical synaptic transmission in goldfish cranial motor nuclei. *J Comp Neurol* **224**, 425–436.

Hackett JT, Cochran SL & Greenfield LJ Jr (1989). Quantal transmission at Mauthner axon target synapses in the goldfish brainstem. *Neuroscience* **32**, 49–64.

Hackett JT & Faber DS (1983*a*). Mauthner axon networks mediating supraspinal components of the startle response in the goldfish. *Neuroscience* **8**, 317–331.

Hackett JT & Faber DS (1983*b*). Relay neurons mediate collateral inhibition of the goldfish Mauthner cell. *Brain Res* **264**, 302–306.

Hansen SB, Sulzenbacher G, Huxford T, Marchot P, Taylor P & Bourne Y (2005). Structures of *Aplysia* AChBP complexes with nicotinic agonists and antagonists reveal distinctive binding interfaces and conformations. *EMBO J* **24**, 3635–3646.

Hartzell HC, Kuffler SW & Yoshikami D (1975). Post-synaptic potentiation: interaction between quanta of acetylcholine at the skeletal neuromuscular synapse. *J Physiol* **251**, 427–463.

Harvey SC, McIntosh JM, Cartier GE, Maddox FN & Luetje CW (1997). Determinants of specificity for α-conotoxin MII on α3β2 neuronal nicotinic receptors. *Mol Pharmacol* **51**, 336–342.

Hatton GI & Yang QZ (2002). Synaptic potentials mediated by α7 nicotinic acetylcholine receptors in supraoptic nucleus. *J Neurosci* **22**, 29–37.

Hieber V, Bouchey J, Agranoff BW & Goldman D (1990*a*). Nucleotide and deduced amino acid sequence of the goldfish neural nicotinic acetylcholine receptor α-3 subunit. *Nucleic Acids Res* **18**, 5293.

Hieber V, Bouchey J, Agranoff BW & Goldman D (1990*b*). Nucleotide and deduced amino acid sequence of the goldfish neural nicotinic acetylcholine receptor β-2 subunit. *Nucleic Acids Res* **18**, 5307.

Horch HL & Sargent PB (1995). Perisynaptic surface distribution of multiple classes of nicotinic acetylcholine receptors on neurons in the chicken ciliary ganglion. *J Neurosci* **15**, 7778–7795.

Jack JB, Noble D & Tsien RW (1975). *Electric Current Flow in Excitable Cells*. Oxford University Press, London.

Jacob MH & Berg DK (1983). The ultrastructural localization of α-bungarotoxin binding sites in relation to synapses on chick ciliary ganglion neurons. *J Neurosci* **3**, 260–271.

Jacob MH, Berg DK & Lindstrom JM (1984). Shared antigenic determinant between the Electrophorus acetylcholine receptor and a synaptic component on chicken ciliary ganglion neurons. *Proc Natl Acad Sci U S A* **81**, 3223–3227.

Jones S, Sudweeks S & Yakel JL (1999). Nicotinic receptors in the brain: correlating physiology with function. *Trends Neurosci* **22**, 555–561.

Kaiser S & Wonnacott S (2000). α-bungarotoxin-sensitive nicotinic receptors indirectly modulate [³H]dopamine release in rat striatal slices via glutamate release. *Mol Pharmacol* **58**, 312–318.

Kimmel CB, Metcalfe WK & Schabtach E (1985). T reticular interneurons: a class of serially repeating cells in the zebrafish hindbrain. *J Comp Neurol* **233**, 365–376.

Korn H & Faber DS (2005). The Mauthner cell half a century later: a neurobiological model for decision-making? *Neuron* **47**, 13–28.

Lopez MG, Montiel C, Herrero CJ, Garcia-Palomero E, Mayorgas I, Hernandez-Guijo JM *et al.* (1998). Unmasking the functions of the chromaffin cell α7 nicotinic receptor by using short pulses of acetylcholine and selective blockers. *Proc Natl Acad Sci U S A* **95**, 14184–14189.

Loring RH, Dahm LM & Zigmond RE (1985). Localization of α-bungarotoxin binding sites in the ciliary ganglion of the embryonic chick: an autoradiographic study at the light and electron microscopic level. *Neuroscience* **14**, 645–660.

Lukas RJ, Changeux JP, Le Novere N, Albuquerque EX, Balfour DJ, Berg DK *et al.* (1999). International Union of Pharmacology. XX. Current status of the nomenclature for nicotinic acetylcholine receptors and their subunits. *Pharmacol Rev* **51**, 397–401.

Luo S, Kulak JM, Cartier GE, Jacobsen RB, Yoshikami D, Olivera BM & McIntosh JM (1998). α-conotoxin AuIB selectively blocks α3β4 nicotinic acetylcholine receptors and nicotine-evoked norepinephrine release. *J Neurosci* **18**, 8571–8579.

McGehee DS, Heath MJ, Gelber S, Devay P & Role LW (1995). Nicotine enhancement of fast excitatory synaptic transmission in CNS by presynaptic receptors. *Science* **269**, 1692–1696.

McIntosh JM, Dowell C, Watkins M, Garrett JE, Yoshikami D & Olivera BM (2002). α-conotoxin GIC from *Conus geographus*, a novel peptide antagonist of nicotinic acetylcholine receptors. *J Biol Chem* **277**, 33610–33615.

McIntosh JM, Plazas PV, Watkins M, Gomez-Casati ME, Olivera BM & Elgoyhen AB (2005). A novel α-conotoxin, PeIA, cloned from *Conus pergrandis*, discriminates between rat $\alpha9\alpha10$ and $\alpha7$ nicotinic cholinergic receptors. *J Biol Chem* **280**, 30107–30112.

Mike A, Castro G & Albuquerque EX (2000). Choline and acetylcholine have similar kinetic properties of activation and desensitization on the $\alpha7$ nicotinic receptors in rat hippocampal neurons. *Brain Res* **882**, 155–168.

Model PG, Highstein SM & Bennett MV (1975). Depletion of vesicles and fatigue of transmission at a vertebrate central synapse. *Brain Res* **98**, 209–228.

Model PG, Spira ME & Bennett MV (1972). Synaptic inputs to the cell bodies of the giant fibers of the hatchetfish. *Brain Res* **45**, 288–295.

Mogg AJ, Whiteaker P, McIntosh JM, Marks M, Collins AC & Wonnacott S (2002). Methyllycaconitine is a potent antagonist of α-conotoxin-MII-sensitive presynaptic nicotinic acetylcholine receptors in rat striatum. *J Pharmacol Exp Ther* **302**, 197–204.

Nai Q, McIntosh JM & Margiotta JF (2003). Relating neuronal nicotinic acetylcholine receptor subtypes defined by subunit composition and channel function. *Mol Pharmacol* **63**, 311–324.

Nguyen D & Sargent PB (2002). Synaptic vesicle recycling at two classes of release sites in giant nerve terminals of the embryonic chicken ciliary ganglion. *J Comp Neurol* **448**, 128–137.

Nong Y, Sorenson EM & Chiappinelli VA (1999). Fast excitatory nicotinic transmission in the chick lateral spiriform nucleus. *J Neurosci* **19**, 7804–7811.

Papke RL, Meyer E, Nutter T & Uteshev VV (2000). $\alpha7$ receptor-selective agonists and modes of $\alpha7$ receptor activation. *Eur J Pharmacol* **393**, 179–195.

Papke RL & Thinschmidt JS (1998). The correction of $\alpha7$ nicotinic acetylcholine receptor concentration-response relationships in *Xenopus* oocytes. *Neurosci Lett* **256**, 163–166.

Park KS, Cha SK, Kim MJ, Kim DR, Jeong SW, Lee JW & Kong ID (2006). An $\alpha3\beta4$ subunit combination acts as a major functional nicotinic acetylcholine receptor in male rat pelvic ganglion neurons. *Pflugers Arch* **452**, 775–783.

Parker MJ, Zhao S, Bredt DS, Sanes JR & Feng G (2004). PSD93 regulates synaptic stability at neuronal cholinergic synapses. *J Neurosci* **24**, 378–388.

Placzek AN, Grassi F, Meyer EM & Papke RL (2005). An $\alpha7$ nicotinic acetylcholine receptor gain-of-function mutant that retains pharmacological fidelity. *Mol Pharmacol* **68**, 1863–1876.

Roerig B, Nelson DA & Katz LC (1997). Fast synaptic signaling by nicotinic acetylcholine and serotonin 5-HT3 receptors in developing visual cortex. *J Neurosci* **17**, 8353–8362.

Sabatini BL, Maravall M & Svoboda K (2001). Ca^{2+} signaling in dendritic spines. *Curr Opin Neurobiol* **11**, 349–356.

Sahibzada N, Ferreira M Jr, Williams B, Wasserman A, Vicini S & Gillis RA (2002). Nicotinic ACh receptor subtypes on gastrointestinally projecting neurones in the dorsal motor vagal nucleus of the rat. *J Physiol* **545**, 1007–1016.

Sargent P (2009). Nicotinic receptors concentrated in the subsynaptic membrane so not contribute significantly to synaptic currents at an embryonic synapse in the chicken ciliary ganglion. *J Neurosci* **29**, 3749–3759.

Shao Z & Yakel JL (2000). Single channel properties of neuronal nicotinic ACh receptors in stratum radiatum interneurons of rat hippocampal slices. *J Physiol* **527**, 507–513.

Shoop RD, Chang KT, Ellisman MH & Berg DK (2001). Synaptically driven calcium transients via nicotinic receptors on somatic spines. *J Neurosci* **21**, 771–781.

Shoop RD, Martone ME, Yamada N, Ellisman MH & Berg DK (1999). Neuronal acetylcholine receptors with $\alpha7$ subunits are concentrated on somatic spines for synaptic signaling in embryonic chick ciliary ganglia. *J Neurosci* **19**, 692–704.

Szabo TM, Weiss SA, Faber DS & Preuss T (2006). Representation of auditory signals in the M-cell: role of electrical synapses. *J Neurophysiol* **95**, 2617–2629.

Tan W, Du C, Siegelbaum SA & Role LW (1998). Modulation of nicotinic AChR channels by prostaglandin E2 in chick sympathetic ganglion neurons. *J Neurophysiol* **79**, 870–878.

Thinschmidt JS, Frazier CJ, King MA, Meyer EM & Papke RL (2005). Medial septal/diagonal band cells express multiple functional nicotinic receptor subtypes that are correlated with firing frequency. *Neurosci Lett* **389**, 163–168.

Titmus MJ & Faber DS (1987). Alteration of identified output synapses spared by axotomy. In *20th Anniversary Commemorative Symposium*. University of Puerto Rico, Institute of Neurobiology, San Jaun, Puerto Rico.

Ullian EM, McIntosh JM & Sargent PB (1997). Rapid synaptic transmission in the avian ciliary ganglion is mediated by two distinct classes of nicotinic receptors. *J Neurosci* **17**, 7210–7219.

Waldeck RF, Pereda A & Faber DS (2000). Properties and plasticity of paired-pulse depression at a central synapse. *J Neurosci* **20**, 5312–5320.

Weiss SA, Zottoli SJ, Do SC, Faber DS & Preuss T (2006). Correlation of C-start behaviors with neural activity recorded from the hindbrain in free-swimming goldfish (*Carassius auratus*). *J Exp Biol* **209**, 4788–4801.

Whiteaker P, Christensen S, Yoshikami D, Dowell C, Watkins M, Gulyas J *et al.* (2007). Discovery, synthesis, and structure activity of a highly selective $\alpha7$ nicotinic acetylcholine receptor antagonist. *Biochemistry* **46**, 6628–6638.

Williams BM, Temburni MK, Levey MS, Bertrand S, Bertrand D & Jacob MH (1998). The long internal loop of the $\alpha3$ subunit targets nAChRs to subdomains within individual synapses on neurons *in vivo*. *Nat Neurosci* **1**, 557–562.

Wonnacott S, Barik J, Dickinson J & Jones IW (2006). Nicotinic receptors modulate transmitter cross talk in the CNS: nicotinic modulation of transmitters. *J Mol Neurosci* **30**, 137–140.

Yu CR & Role LW (1998). Functional contribution of the $\alpha7$ subunit to multiple subtypes of nicotinic receptors in embryonic chick sympathetic neurones. *J Physiol* **509**, 651–665.

Zhang ZW, Coggan JS & Berg DK (1996). Synaptic currents generated by neuronal acetylcholine receptors sensitive to α-bungarotoxin. *Neuron* **17**, 1231–1240.

Zhang ZW, Vijayaraghavan S & Berg DK (1994). Neuronal acetylcholine receptors that bind α-bungarotoxin with high affinity function as ligand-gated ion channels. *Neuron* **12**, 167–177.

Zottoli SJ (1977). Correlation of the startle reflex and Mauthner cell auditory responses in unrestrained goldfish. *J Exp Biol* **66**, 243–254.

Author contributions

C.L.G., T.M.S., J.M.M. and D.S.F. designed the research; C.L.G., T.M.S., S.C.D. and R.F.W. performed the experiments; J.M.M. contributed analytical tools; C.L.G., T.M.S., J.M.M., S.C.D., R.F.W. and D.S.F analysed and interpreted data, C.L.G. wrote the paper with critical input from T.M.S., J.M.M. and D.S.F. All authors were involved in the design or analysis of experiments and in the critical reading and revision of the manuscript. All have approved the final version of the paper. The experiments were done at the Department of Neuroscience, Albert Einstein College of Medicine.